Title

THE IDENTIFICATION OF NEW ASTATINE ISOTOPES USING THE GAS-FILLED MAGNETIC SEPARATOR, SASSY

Author

Yashita, S.

Publication Date

1984-02-01

Lawrence Berkeley Laboratory
UNIVERSITY OF CALIFORNIA

THE IDENTIFICATION OF NEW ASTATINE ISOTOPES USING THE GAS-FILLED MAGNETIC SEPARATOR, SASSY

S. Yashita
(Ph.D. Thesis)

February 1984

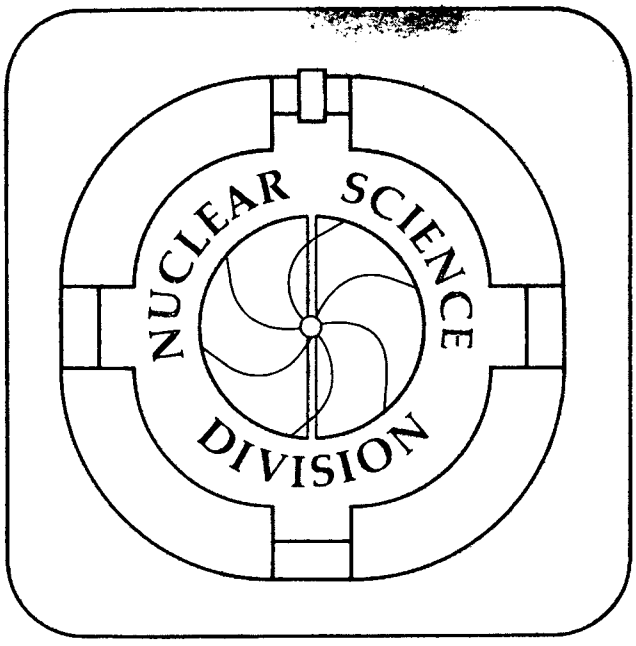

Prepared for the U.S. Department of Energy under Contract DE-AC03-76SF00098

DISCLAIMER

The Identification of New Astatine Isotopes Using the Gas–filled Magnetic Separator, SASSY

Saburo Yashita

Lawrence Berkeley Laboratory

University of California, Berkeley

Berkeley, California 94720

ABSTRACT

A He-filled on-line mass separator system was built at the SuperHILAC and used to study the fusion products in the reaction $^{56}Fe+^{141}Pr$. The new neutron-deficient isotopes ^{194}At and ^{195}At were produced in this bombardment as three- and two- neutron-out products, respectively, and were identified by the α-α time-correlation technique. The measured α energies and half lives are 7.20±0.02 MeV and 180±80 msec for ^{194}At, and 7.12±0.02 MeV and 200±100 msec for ^{195}At.

ACKNOWLEDGMENTS

It has been a great privilege and joy to be among the gifted scientists during my years in the University of California and Lawrence Berkeley Laboratory.

Willard Libby who emphasized the enjoyment of science in that special atmosphere of creativeness and originality which always surrounded him, stimulating and nourishing the minds of all, will always remain in my memory.

Glenn Seaborg provided a near ideal environment throughout my graduate years with challenging subjects. He allowed me to work amongst his best colleagues and scientists gathered from other institutions and abroad.

Albert Ghiorso, project leader of SASSY, has the gift of magic to conquer the mysterious and unsavory side of experimental science and somehow transforms seemingly impossible projects into possible ones. His keen intuition, vast experience, brazenness and tireless drive to accomplish this task simply have to be seen to be believed.

Naturally a project of this size and complexity requires more than one man's effort. The following dedicated people are heavily involved in the support of this project in their fields of expertise in order to materialize the ideas in the mind of Al Ghiorso into a reality.

Rich Leres managed the computer system as flawlessly as he plays with his other favorite games.

Matti Leino, man of truth and reliability, reduced the data with ultimate precision. I did not have a chance to verify his statement that girls in his home land, Scandinavia, are the prettiest in the world.

Ken Ransdell fabricated the mechanical assembly with care and precision, and even painted it with Blue and Gold.

Al Wydler constructed the bullet proof electronics for the detectors. Although he claims that electronics is a pure science, I am not throughly convinced of this from the way he works.

Other people who have lent their support to this work include L. Archambault and G. Hartley, not to mention the crews at the SuperHILAC. Constructive comments were received from H. Gould, J. Nitschke, S. Prussin and J. Rasmussen who kindly read this manuscript. They are gratefully acknowledged.

This work was supported by the Director, Office of Energy Research Division of Nuclear Physics of the Office of High Energy and Nuclear Physics of the U.S. Department of Energy under Contract No. DE-AC03-76SF00098.

TABLE OF CONTENTS

I. INTRODUCTION

Often scientific knowledge can be obtained and advanced only after a series of scientific and technical barriers are overcome with much patience. The Curies, pioneers in nuclear chemistry, obtained polonium after incomparable effort and determination [1]. Continuous progress in understanding the subatomic world has been taking place throughout this century in the hands of dedicated people [2]. Among such developments, the searches for and the studies of unstable nuclides certainly have been undertaken just as enthusiastically as in the earlier days utilizing the foremost techniques available at the time, and we have come to know the existence and the properties of more than 2000 nuclides [3-5]. By far the most effective means to produce heavy nuclides today is to obtain them as fusion residues in heavy ion reactions [6]. The development of heavy ion accelerators which are suitable for inducing such reactions in recent years has been remarkable, and machines which are capable of accelerating any elements up to uranium with sufficient energy and intensity are now available [7]. The great instability of nuclides expected to be produced by their usage naturally calls for far improved capabilities of detector systems in turn [8,9]. To meet this requirement, we have constructed the detector system SASSY (Small Angle Separator SYstem) based on the principle of the gas-filled magnetic separator, emphasizing detection speed with a minimal sacrifice in detection efficiency. The equipment has been operated for heavy elements including trans-actinides with respectable projectile rejection of $1{:}10^{12}$ while maintaining 35 percent transmission for fusion residues. The time required for this separation is in the order of one microsecond for the typical fusion residues of our concern, and consequently the activities whose half life are in this order can be studied by this equipment.

It was an amusing coincidence that the first new nuclide detected in the SASSY testing stage was an isotope of polonium, differing from the Curies' original by 18 neutrons [10]. As a natural extension, we began searches for new isotopes in the nearby region. In the Po work, unfortunately, the large electron capture branch as well as the relatively long α half life of the daughter ^{188}Pb, made the genetic α-α time correlation method difficult for the assignment purpose in our equipment. Learning from this experience, we proceeded with the experiment described in this work keeping the necessary properties of the daughter for correlation work in mind. As a result, we identified ^{194}At and ^{195}At positively by genetic α-α correlation [11]. The experimental procedure and the properties of isotopes produced as well as the configuration of the first operating detector system used until the early part of 1982 are described.

II. EXPERIMENTAL APPARATUS

A. General concept

Our detector system consists of beam line, target section, dipole magnet, quadrupole doublet and detectors with their electronics, when it is viewed sequentially from upstream (Fig.1). It measures 4.0 m from target to focal plane and the entire system downstream from the target is filled with 1.0 torr He gas. Projectiles accelerated in the SuperHILAC first collide with a thin target of less than 1.0 mg/cm^2. Fusion residues emitted close to 0 degrees, keeping their specific momentum obtained in the collision [12], will be greatly separated from projectiles and scattered target atoms according to the differences in their magnetic rigidities, while they traverse through the gas-filled dipole magnet. They are then focused in the quadrupole magnet onto the focal plane further down stream where the electronic detectors are located. This massive quadrupole section also serves as an effective shield for the following detector section against the high background noise generated at and around the target area. The processes up to this point can be regarded as a stage of filter [13], whose purpose is to suppress an otherwise overwhelming background, such as projectiles, to a level tolerable for the subsequent electronic detectors while allowing the fusion residues to pass through freely. The ion-optics have been designed with the aid of code BELIN [14], and one of the calculations which indicate the focusing characteristic of the optics is shown in Fig. 2. The separation speed is determined by the flight time of the fusion residue from the target to the detectors, and for the reaction used in this work it is 0.5 μsec.

The fusion residues and the few background particles which manage to pass through the magnetic optics then go through time of flight detectors for their velocity measurement and finally implant themselves into an array of surface barrier detectors for measurement of total kinetic energy and studies of

subsequent alpha decay, if any. The velocity and kinetic energy information are effectively used to further discriminate fusion residues from background particles in the data reduction stage, and final assignment of nuclides is made by use of α energies and their genetic time correlations whenever possible.

B. Beam line and target section

The projectiles from the accelerator go through the beam line before reaching the target section. While the primary function of this section is to give the projectiles the final tuning so that they form the 6 mm diameter circular image over the target, the following devices to control projectile characteristics have been installed as well. A set of Al foils next to the target can degrade the projectile energy by small steps and a series of heavily copper-plated electromeshes 1 m upstream from the target attenuate the projectile intensity when the energy measurement has to be performed at the surface barrier detector in the dipole magnet. The beam wobbler 1.5 m upstream from the target, made from a 3 phase motor winding, continuously displaces the beam image over the target in circular fashion to prevent hot spots from the beam being too concentrated, thus allowing the target to withstand a higher average flux. Although the pressure of this section is normally kept below 10^{-6} torr by differential pumping, any pressure surge detected at the vicinity as an indication of window breakage triggers a local "slammer" valve within 20 msec to protect the accelerator from a helium surge or from broken target fragments.

The target and the beam window located at the entrance of the dipole magnet separates the He gas from the vacuum in the beam line. The vacuum tight beam window and target with its backing are mounted at the end of a cylindrical block which is inserted in the target chamber as a unit. Cold nitrogen gas from an LN tank is introduced to the 3 mm space between the beam window and the target to cool their inner faces continuously during bombardment.

C. Magnetic system

The entire magnetic system, dipole and quadrupole sections, including the detector section, is completely filled with the He gas. To ensure the purity of He gas in the magnetic system, a controlled amount of high grade He is introduced continuously in the dipole magnet close to the target section and is exhausted at the location close to the focal plane of SASSY. The exit gas is continuously pumped away by an Heraeus pump. The He pressure is maintained well within 1 percent of the desired value by use of a needle valve at the injection point actuated by an MKS Baratron. For the beam intensity measurement, we electrically insulated the entire chamber between the dipole gap to make it act as a faraday cup.

1. Dipole magnet

The dipole magnet produces up to 12 kgauss of homogeneous magnetic field in its 7.0 cm pole face gap. The 90 cm effective length is enough to give a 23 degree deflection to the heaviest element. The principle of operation of gas-filled separators resembles in certain ways that of the more familiar β spectrometers which are momentum separators for electrons. The equation of motion of an ion, with its mass m and charge q moving with velocity v perpendicular to the applied homogeneous magnetic field B, is common to all magnetic separators of this type and is given by the following expression [15].

$$B\rho = \frac{mv}{q} \tag{1a}$$

where the left hand term, commonly referred to as magnetic rigidity, which is the product of the applied magnetic field strength B and the radius of curvature of the moving ion ρ, implies a direct measure of the quantity to the right, that is momentum, mv, divided by the charge q. Whereas in an electron spectrometer which operates *in high vacuum*, the magnetic rigidity becomes a

linear measure of the electron's momentum due to the known value of electron charge q_e, in an ion separator operated in a similar manner, this simple conclusion unfortunately can not be drawn. This is because the ionic charge q_{ion} generally is not a single valued quantity but rather various integral multiples of q_e. The unpredictability of q_{ion} in vacuum, for example, stems from its sensitivity to the subtle variation of the medium where each ion happens to pass before its entrance to the vacuum, such as the chemical and physical characteristics of the target and even to the way it is produced, that is the nature of the nuclear reaction involved. This large fluctuation in q_{ion} seriously impedes the transmission efficiency as well as literally destroying the function of the separator. The way to greatly reduce this q_{ion} variation without slowing down the separation speed appreciably is to fill the dipole magnet gap by a thin gas of appropriate composition and pressure [16,17]. The various integer-valued charge states then become a well defined distribution characterized by the mean charge state $\bar{q}$, due to the large number of charge-changing collisions the ions experience with the surrounding gas atoms. If we represent this equilibrated distribution by its average charge value $\bar{q}$, Eq.1a will be replaced by

$$B\rho = 22.7\times10^3 \frac{A\,v/v_0}{\bar{q}(Z,A,v,Z_m,A_m,p)}\ gauss\cdot cm \qquad (1b)$$

expressed in atomic units with Z,Z_m,A,A_m the atomic number and mass of ion and gas respectively , p pressure of the gas and v_0= c/137 (2.18×10^8 cm/sec). If we use the following widely used one-parameter semiempirical expression which applies adequately to the gaseous medium for $\bar{q}<0.3\times Z$ [18],

$$\frac{\bar{q}}{Z} = \alpha \times \frac{v}{v_0} Z^{-\frac{1}{2}} \qquad (1c)$$

where α is an open parameter, and recognize that

$$Z = \frac{A}{1.98+0.0155A^{\frac{2}{3}}} \approx \frac{A}{2.5}$$

the Eq. (1b) becomes

$$B\rho \propto A^{\frac{1}{2}}$$

which indicates that the magnetic rigidity indeed becomes a measure of mass A as long as *Eq. 1c holds reasonably well*, and this furnishes the basic operational principle of ion separation.

2. Experimental determination of magnetic rigidities

As we have seen in the previous section, our primary concern now is to know the dependence of $\bar{q}$ on Z, A, v, Z_m, A_m, p with greater accuracy, which is most crucial for the successful operation of the separator. This dependence has been extensively studied for fission fragments [19,20], and various theoretical and multi-parameter semiempirical formulas [21-23] have been suggested for its prediction. For lanthanide elements, however, a departure from these predictions was observed, suggesting the stronger role of the atomic shell effects in the velocity range of our concern [24-26]. Since this discrepancy is likely to exist for higher Z elements and its magnitude was difficult to ascertain a priori by existing theories, we decided to obtain the values of magnetic rigidities for heavy elements, including trans-uranium elements, empirically.

We used 1.0 torr of He as the filling gas as usual and elastically scattered various target atoms ranging from Sm (Z=62) to Cm (Z=96) with ^{20}Ne and ^{40}Ar beams from the SuperHILAC to obtain values of B which made them traverse the optical axis. To minimize the velocity dispersion in the target, most of the non-radioactive targets were made by sputtering from their metal foils, and their thicknesses were kept below 50 $\mu g/cm^2$. The radioactive ones were prepared by electrodeposition.

As for the choice of the filling gas Z_m, we used He exclusively in our experiments. This is because magnetic rigidities of ions in He have been observed to be relatively independent over a wide range of ion velocities [19], and its low Z discourages multiple-scattering of ions, which would lower the high transmission efficiency of the separator [27]. The gas pressure p has been known to affect the resolution of the separator significantly, largely through two counteracting aspects [19]. Although higher pressure contributes to better resolution through a narrower charge distribution width because of an increased number of charge changing collisions, excessive pressure will lead to a rapid increase in multiple scattering which hinders the resolution. Therefore one needs to determine the optimum pressure for the experiment. We studied this effect in the reaction $^{48}Ca+^{166}Dy$, and determined the optimum value to be 1.0 torr. The transmission efficiency at this condition was measured to be 35 percent by directly comparing the activity caught immediately after the target with that collected at the focal plane. The full widths at half maximum of the image size at the focal plane were 7.5 cm, horizontally, and 2.2 cm, vertically.

As a result, the values of magnetic rigidities obtained for each element are plotted as according to Z in Fig. 3. For comparison, a prediction by Eq. 1c is plotted as a dashed curve, using α=0.28 to fit the data. Whereas the prediction by Eq. 1c represents the general trend of magnetic rigidity well, one may notice the periodic fluctuation of experimental values. Although this discrepancy can be partly explained by the introduction of Bohr-Lamb criteria [22], which take into account the ionization energy of the most losely bound outer electron in the ion, the rather serrated dependence obtained using the relativistically corrected Hartree Fock calculation [28,29] as compared to the smoother appearance of the empirical result suggests a significant contribution from inner electrons to the mean charge $\bar{q}$. A refinement to account for this behavior is under way [30].

D. Detectors and electronics

The detector section to study neutron deficient astatine isotopes is set up with a pair of avalanche counters for the time of flight measurement and an array of ten silicon surface barrier detectors at the focal plane (Fig. 4). The fusion residues are embedded near the surface and their total kinetic energy at impact as well as the energy of successive α decays and their event times are recorded on magnetic tape by a PDP15 computer.

1. Avalanche counters

A pair of position-sensitive avalanche counters, similar to the one described in Ref. 31, were constructed for the time-of-flight measurement. Each has effective area of 8.9 by 17.8 cm and they are placed 122 cm apart. A counter consists of a center tungsten mesh anode, which collects fast moving electrons for timing signals, and two silver coated formvar windows, which act as cathodes and enclose the counter gas, pentane. Silver is evaporated in striped fashion, one vertically and the other horizontally for two dimensional position sensitivity. By connecting these stripes to a resistor chain and taking the amplitude ratio of the pulses extracted from each end of the chain, the position of ion passage is obtained. The 8 mm spacing between the windows is filled with pure pentane gas, slowly introduced from the bottom and exhausted at the top, maintaining the pressure equilibrium between the pentane and He outside. This procedure reduces the strain on thin windows ($<15\ \mu g/cm^2$), which are constructed to be as thin as possible for the reduction of ion scattering. The timing resolution is less than a nano second which amounts to less than 1 percent of the velocity of our fusion residues. The position resolution is about 6 mm which is the spacing of the silver stripes and this value is better than the magnetic rigidity resolution.

2. Surface barrier detectors

A horizontal array of ten 21 by 13 mm rectangular silicon surface barrier detectors is placed at the focal plane. In order to minimize the detection inefficiency, which comes from the detector casing and inactive edges, they are arranged to overlap their borders. The energy resolution was 50 keV for α particles and about 15 percent for the 50 MeV recoils.

3. Electronics

All information processed in the SASSY electronics can be divided into either analog or digital information (Fig. 5). The analog information consists of α, recoil or fission energy from the surface barrier detectors and the time of flight, the position and the energy loss from the avalanche counters. This is first serially converted by a multiplexer and then sequentially digitized by an ADC and finally sent to the PDP15 through an interface. The digital information consists of the crystal identification numbers, the millisecond clock which records the time from the beginning of the experiment, and the microsecond clock which resets at every beam burst of the SuperHILAC. All events which take place in the SASSY detectors are tagged by these two clocks. This digital information is fed directly into the interface together with the corresponding analog information. Since the system dead time, which mainly comes from the time required for the sequential digitization of analog signals, exceeds 400 μseconds for each event, we installed an additional ADC and a microsecond clock which independently processes the α signals whenever the main ADC is busy. This auxiliary circuit helps to reduce the detector dead time down to 3 μsec for α particles, and together with the gas-filled separator front end makes it possible to truly detect nuclides whose half lives are in the order of microseconds.

III. DATA HANDLING

A. On–line monitor

While all data fed into the computer are stored on standard magnetic tapes for complete reduction after the experiment, the capability of an immediate access to most of data through a CRT screen has been valuable. This on-line monitor was used for the energy calibrations of the detectors prior to each experiment. During the experiment, we monitor its progress, as well as the state of the operation of each component, for fast corrective action if necessary. The data monitored at present are α, recoil and fission energy spectra from each surface barrier detector, vertical and horizontal location as well as dE/dZ of ions which go through the avalanche counters, the time of flight spectra, and delayed α spectra. We can construct a two dimensional plot from any two parameters listed above, with arbitrarily set channel windows in each of the parameters. This helps us to analyze an event using several characteristics recorded in different detectors. For example, the two dimensional plots made up with the time of flight and the recoil energy were used extensively to differentiate true fusion recoils from various backgrounds.

B. Off–line data reduction

Mainly due to the memory size limitation of the computer, all of the information which involves the time correlations have to be extracted off-line from magnetic tapes. At this stage of data reduction, all spectra are handled in the full 1024 channel resolution as they are stored in the memory, and they are individually gain shifted by internal and external calibration sources. The presently available off-line programs are ones which produce α spectra with gain correction, a α-recoil time-correlation program which looks for fusion recoil candidates preceding specified α events, and an α-α time-correlation program which searches for daughter α candidates following the specified α

mother.

When these time-correlation programs are used, the existence of the accidental correlations and their consequences, in particular, the effect to the apparent half life obtained from the raw data, have to be considered. The accidental correlation inevitably arises due to our uncertainty when we pick the correlation pair in the environment where background and interference exist. For example, we adopted the convention of searching for the correlation pair which satisfies the requirements *with the shortest time interval between the two*. There is, of course, no guarantee we select the truly correlated pair by this method. In fact, there are two sources of error which can be readily considered. One is caused by missing the true mother, for example due to the system dead time, and the other is caused by a not truly correlated event taking place in between the true pair as an interference. The effect can be significant especially in the α-recoil correlations where the recoil rate is high.

As an example, we consider a case where we have an α event and look for a possible mother recoil. $I(t)dt$, which is the differential probability of finding a mother candidate in dt with time t before the α event, will be given by the following expression,

$$I(t)dt = ke^{-\lambda t}P(0)\lambda dt + ke^{-\lambda t}P(0)rdt + (1-k)P(0)rdt \qquad (2a)$$

where k is the efficiency of the detector system, λ the decay constant of the mother, and r the recoil rate of possible mother candidates. If we assume the recoils are randomly distributed, $P(0)$ which is the probability of finding no recoil over an interval of time t, will be the Poisson distribution [32],

$$P(0) = \frac{(rt)^0 e^{-rt}}{0!} = e^{-rt}$$

and Eq. 2a will become,

$$I(t)dt = ke^{-\lambda t}e^{-rt}\lambda dt + ke^{-\lambda t}e^{-rt}rdt + (1-k)e^{-rt}rdt \qquad (2b)$$

The first term on the right is the probability of finding the true mother, the second that of finding the wrong mother due to the random event taking place after the true mother event, and the last term that of finding the wrong mother due to the real mother being not detected at all because of the system dead time. The final decay formula can be obtained from Eq. 2b

$$\frac{dN}{dt} = I(t)N_a = kN_a(\lambda+r)e^{-(\lambda+r)t} + (1-k)N_a r e^{-rt} \qquad (3)$$

This means we need two corrections to the raw data in order to obtain the true decay constant λ for the mother. First we subtract the effect from the second term of this expression, which appears as a long lived component in the raw data, and obtain λ_{obs}. Finally we obtain the true decay constant, λ, according to,

$$\lambda_{obs} = \lambda + r \qquad (4)$$

In α-α correlations, while this last correction is often negligible due to the low rate of α events, the events, which escaped the detection due to the 2 π geometry of the α detectors, are equivalent to having the large system dead time, and will possibly lead to significant amount of accidentals. Therefore the number of the accidental events, which is vital for the assignment of nuclides based on the genetic α-α correlations, must be estimated.

When we express the probability of finding n accidental events in time t after a mother event by $P(n)$, the probability of finding any number of accidentals will be expressed as follows, assuming the Poisson distribution,

$$P = P(1) + P(2) + \cdots = e^{-R}(R + \frac{R^2}{2} + \ldots) = 1-e^{-R} \qquad (5)$$

$$R = \frac{N_d}{T} t$$

where N_d is the number of events in the daughter channels, t is the search time used for the correlation, and T is the duration of the experiment. Therefore,

the total number of accidentals, N_{acc}, for a N_m mother will be,

$$N_{acc} = N_m(1 - e^{-R}) \tag{6}$$

This formula will be reduced to the familier expression [33],

$$N_{acc} = \frac{N_m N_d}{T} t \tag{7}$$

if $R<<1$. Finally for the detector array used in this experiment, the total accidentals are the sum of accidentals in each individual detector as calculated above.

IV. EXPERIMENT

A. Strategy

When we attempt to synthesize new nuclides, there are generally three areas of concern which can make experiments difficult, namely production cross section, decay mode and half life of the nuclide. Especially when the accelerator availability is limited, each of these points has to be considered carefully. Fortunately, due to the fast detection speed of our equipment, the half life of nuclides did not arise as a serious threat. In fact, we experienced cases where shorter lived nuclides can be identified more positively. Therefore we focus on the optimization of the production cross section and identification efficiency through the selection and the production methods for nuclides.

1. The choice of nuclide to be produced

For practical and realistic reasons, we allow ourselves the consumption of approximately one shift (8 hours) worth of accelerator time to identify each new nuclide. This consideration just about excludes all those unstable against β, γ or fission as far as the choice of nuclides are concerned, either due to the lack of the signature the radiation provides or the inability to obtain a highly efficient electronic detector for the radiation [34]. Even among the remaining α emitting nuclides, which populate themselves on the neutron deficient side of elements ranging from lanthanides to trans-actinides, those at neither the high nor low Z end will be promising candidates when their production cross sections are considered. This situation can be illustrated, for example, by plotting the proton binding energies and fission barriers [35] for the lightest known nuclides of this region (Fig. 6). The rapid fall-off of fission barriers for Z above 90 implies severe fission competition [36] and the negative proton binding energies appearing towards the low Z elements indicate that nuclides of this region have been well searched for already. So our choice narrows down to the region

of the neutron deficient α emitters of moderately heavy elements [37-40]. Among these α emitters, those with non α-active daughters need to be assigned by, an argument such as, the shape of the excitation function used in our previous Po work. It has to be realized, however, the construction of a convincing excitation function does require the accumulation of a relatively large number of α events for several bombarding energies, which naturally requires the extended bombardment time.

Ultimate confidence in an assignment, as well as the reduction of the duration of the bombardment, can be achieved when we select an unknown α emitter whose daughter is a known α emitter. If one can establish the genetic correlation between them, very few valid events are necessary for a positive assignment [41]; in fact, in the recent discovery of one atom of element 109 at GSI, the time correlation of a single decay chain was used as a valid argument [42]. When the limitation of the apparatus is considered, however, we realize that only carefully selected mother-daughter pairs can be successfully assigned by this method. This is because the validity of the assignment will be based on a statistical argument, such as whether the number of the observed correlations is significant or not when the accidental correlations are taken into account. Therefore we are required to invest special effort in reducing the number of the accidentals to obtain meaningful results.

As obtained earlier, the value of the accidental correlation N_{acc} is given by Eq.7. Since N_{acc} is proportional to N_m, N_d and t, the number of events in the mother channels, those in the daughter channels, and the search time, and inversely proportional to T, the duration of the experiment, we should minimize N_m,N_d and t, and maximize T to reduce N_{acc}. Although T is determined by the accelerator time for this type of experiment and can not be altered in practice, N_m,N_d and t can certainly be minimized by the appropriate selection of the mother-daughter pair, the nuclear reaction involved, the experimental

procedure and the detector array characteristics. The selection of a short half-lived daughter, for example, allows us to use a correspondingly short search time t, which is advantageous. N_m and N_d can be minimized by selecting a mother and daughter whose α energies are unique among the neighboring nuclides, and by chosing nuclear reactions which do not produce a large amount of the daughter nucleus directly via αn-out reaction channels. The use of high purity targets, both chemically and isotopically, also helps to reduce the direct production of the daughter by unwanted reaction channels, and reduces as well the possibility of creating nuclides whose α energies might interfere with the nuclides in question. The use of high energy resolution detectors, which allows a narrow α energy window, and position sensitive detectors, which effectively reduce the size of the individual detectors to that of their spatial resolution, can reduce N_m and N_d [39,40].

As a final choice of nuclide, neutron deficient astatine isotopes were selected. Their proton binding energies indicate moderate stability against proton emission and their relatively high fission barrier of 10 MeV should ensure suitable production cross sections. In particular, ^{194}At is recognized as possessing the ideal characteristics for α-α time-correlation work. Its daughter ^{190}Bi does have a large α branch with a unique energy among its neighbors and its relatively short half life (<10 sec) can be handled comfortably by the experimental apparatus.

2. The choice of the nuclear reaction to be employed

There are three reasons that ^{56}Fe+^{141}Pr was chosen over the conventional reactions with Ne projectiles where light astatine isotopes have been produced in reactions involving a large number of evaporated neutrons [43]. First a weakly excited and rather neutron-deficient compound nucleus is formed in this reaction. This low excitation energy is known to be advantageous to optim-

ize the production cross section where the neutron evaporation has to compete against other reaction channels [44,45] such as charged particle emissions in this highly neutron deficient region [46-48]. Second, this low excitation energy discourages the production of a large number of unwanted nuclides by limiting the energy available for these reaction channels, thus reducing the number of accidental correlations. Third, the higher velocity fusion residues in this reaction reduce the effect of multiple-scattering in the gas filled separator and cause it to operate with higher efficiency.

To select the best target projectile combination from the limited data we had, all stable nuclides whose natural abundance exceed 1 and 5 percent for target and projectile, respectively, and yield ^{197}At as a compound nucleus were selected as the feasible candidates. The excitation energies when these combinations are fused at energies corresponding to their coulomb barriers were obtained using nuclear proximity potentials [49,50] and Q values from Ref. 35 then plotted as the dashed line in Fig. 7. The ones which include the extra energy expressed in Ref. 51 are shown in the figure as the solid line. The projectile Fe and its associated target Pr can be seen as one of the best combinations for the attainment of low excitation energy.

B. Experimental procedure

1. Target preparation

Since ^{141}Pr is the only stable isotope, the possibility of nuclide production from isotopic impurities was eliminated. Small Pr fragments were cut from a chemically pure metal block and vacuum evaporated in a tungsten boat onto a 1.85 mg/cm^2 Havar target backing foil. Since relatively fast oxidation was anticipated [52], the evaporation took place shortly before the experiment and the finished 600 $\mu g/cm^2$ target was stored in an Ar atmosphere until the bombardment. We used a 1.85 mg/cm^2 Havar foil for the beam window of this

experiment. The 3 mm space between the target and the beam window was swept by a continuous flow of nitrogen gas, for cooling, during the bombardment.

2. Projectiles

^{56}Fe projectiles were delivered from the SuperHILAC at 34 pulses/sec with a beam width of 3.5 msec. The beam energy was measured to be 280 MeV out of the accelerator and its half width was 2 MeV. We obtained an average of 10^{11} ions/sec during the bombardment. Energy was changed by replacing the Al degrader foils in the beam line. The optimal energy for the isotope production was determined from the prediction of the neutron evaporation code JORPLE [53].

3. Magnetic optics

Since we were searching for considerably neutron deficient astatine isotopes, a mass correction to the value of the previous magnetic rigidity calibration for β-stable isotopes (Fig. 3) was necessary. Obtaining A=211 to be a β stable form of At by Green's expression [54], the mass ratio of the expected nuclide, ^{194}At to this value, ie. 194/211, was multiplyed by the $B\rho$ value found in Fig. 3, and the magnetic field strength was reduced accordingly. Since we located the fusion residues and their α activities in the avalanche counters and surface barrier detector array approximately at the optical axis, no further adjustment of the magnetic field strength was carried out.

Our standard 1.0 torr He pressure was used in this experiment. The detector system efficiency should be close to the optimum value at this pressure. This is based on studies, of the pressure effects on the efficiency in the reaction ^{48}Ca+^{164}Dy, done before this experiment.

4. Detector calibration

Prior to the experiment, the surface barrier detectors were calibrated by a ^{212}Pb-^{212}Bi-^{212}Po source for α energies and by a ^{252}Cf source for the recoil and fission energies. The time-of-flight system was also calibrated by the ^{252}Cf source.

V. RESULTS

A. The identification of ^{194}At

To establish the production of ^{194}At as well as to obtain its properties, various on-line and off-line codes mentioned earlier were used. To give a clear picture of what took place in our detector system, and how these codes were used, we here present in detail the events in sequential order as they appeared in the electronic detectors, using the case of ^{194}At as an example. The experiment was carried out at a projectile energy of 255 MeV in its laboratory frame.

1. Time-of-flight spectra

All ions which traverse the magnetic optics appear first at the time-of-flight (TOF) detectors as in Fig. 8. In this reaction there are three peaks observed. The one around 150 nsec strongly suggests the presence of the fusion residues, where their TOF was calculated to be 144 nsec for the compound nucleus ^{197}At. This, however, does not necessarily indicate the production of the new isotope, which is expected to be produced as an xn-out product since other charged-particle-out products, such as p- and α- out products, have a flight time similar to the xn-out case. The highly attenuated projectiles and scattered target atoms can be observed in the spectra also. The projectile rejection at this bombarding energy is 3.6×10^{12}:1.

2. Recoil energy spectra

After the passage through TOF detectors, the recoil ions implant themselves into the surface barrier detectors where their energies are measured. Better differentiation of fusion residues against the backgrounds can be obtained when this recoil energy information is combined with the previously described TOF spectra. The matched pairs are represented in the two dimensional density plot in Fig. 9, and the gross recoil energy spectra are shown in

Fig. 10. The peak at 70 MeV agrees well with the kinematically required value of 72 MeV for the fusion residues. To ensure this assignment, we correlated the recoils with the 6.84 MeV α events of a known isotope ^{194}Po which was produced abundantly in this reaction as a fusion residue. The resultant strong correlation after the subtraction of accidentals by Eq. 6 clearly indicates the validity of this assignment. For the future α-recoil time-correlation work, the fusion residue candidates are finally defined as the ones which simultaneously satisfy the TOF and recoil energy requirement as indicated in the box in Fig. 9.

3. α spectra

The gain corrected α spectra were obtained by use of the off-line reduction program. Since the fusion residues are embedded in the crystals, α energies obtained from their decays include the energies of the accompanied host nuclei, which recoil in the opposite direction, as well as the α energies. The contribution of this recoil energy unfortunately is not well known, due to the uncertainty of the energy defect, so the final α energy was calibrated internally by prominent α active isotopes ^{191}Bi (6.32 MeV), ^{195}Po (6.61 MeV) and ^{194}Po (6.84 MeV) produced in the bombardment. The resultant α spectrum is shown in Fig. 11. A new 7.20 MeV α line was observed.

4. α–recoil time correlation

To obtain the half life of the nucleus associated with this 7.20 MeV α line, we searched for the recoil candidates which met TOF and energy requirements and preceded the α events by not more than 1.0 sec (Fig. 10). We chose the pair with the shortest time interval when there was more than one candidate, and the result is summarized in Fig. 12. The half life of this activity was determined from these time intervals and was found to be 180±80 msec by the code "Maximum Likely" [55] taking account for the correction (r=0.19/sec) by Eq. 4.

5. α−α time correlation

An α-α time-correlation program was used to determine the daughter of the 7.20 MeV α activity. We searched for all α events that occurred within 10 sec after the mother events. Fig. 13 shows the result of this search. Since they contain accidental correlations, we must estimate their magnitudes. We calculated the accidentals by Eq. 6 for each crystal and their sum is plotted in Fig. 13. It is evident that there are a significant number of 6.45 MeV events greater than the estimated accidentals. From the time intervals of 7.20 and 6.45 MeV events, a daughter half life of 5±2 sec was determined. Recognizing that ^{190}Bi is the only isotope which satisfies these properties, we assign the 7.20 MeV activity to its mother, ^{194}At. Since 8 observed correlations is 3.7 standard deviations away from the estimated accidentals of 2.35, the error probability of these correlations is estimated to be less than 0.1 percent.

B. The identification of ^{195}At

The identical identification procedure as previously described for ^{194}At was carried out for ^{195}At. Another new α line (7.12 MeV) observed at a slightly lower projectile energy of 249 MeV (Fig. 14) was determined to belong to ^{195}At from the observed strong α-α correlations to its known ^{191}Bi daughter energy of 6.32 MeV (Fig. 15). A 13 sec daughter search time was used for this correlation and the resultant 14 correlated events around 6.32 MeV α energy were found to be 3.6 standard deviations away from the estimated accidentals of 5.51, and the error probability of these correlations is estimated to be less than 0.1 percent. The α-recoil code previously used in the ^{194}At case gave the half life of this 7.12 MeV α activity 200 ± 100 msec (Fig. 16).

VI. DISCUSSION AND CONCLUSIONS

The properties of the astatine isotopes identified in this work were examined from the context of the available systematics and predictions. They were then utilized, together with those of known isotopes in this region, to overcome in either straightforward or evasive fashions, the difficulties associated with the production of new nuclides in this region such as instability against proton emission, possible short half life and unmanageably low production cross section. The detector system performance was also evaluated in order to point out the desired improvements which could enlarge its capability.

A. The properties of ^{194}At and ^{195}At

While the α decay energies of ^{194}At and ^{195}At observed in this work agree well with the α energy systematics (Fig. 17), and support the validity of their assignments, they provide an excellent testing ground for the applicability and validity of various nuclear mass predictions [56]. A better mass prediction in turn can be used to determine the location of the proton drip line to greater accuracy as well as to improve the partial α and proton half life predictions and the production cross section estimates, which are all vital for experimentation leading to the future extension of nuclides in this region. As can be seen in Fig. 18, the prediction by Liran and Zeldes agrees very well with the absolute value as well as the trend of α energies of neutron-deficient astatine isotopes. When we calculate the proton binding energies for these isotopes using their mass prediction, it can be seen that protons in ^{194}At as well as ^{195}At are already slightly unbound which suggests a possible proton decay mode for the further neutron deficient At isotopes (Fig. 19). In the context of ease of synthesis, to avoid instabilities against proton emission, we should probably not pursue odd-proton nuclei of astatine isotopes much farther but shift our emphasis to

even-proton nuclei like radon where the proton drip line extends down to A=193. In the following half life and cross section predictions, the calculations for Rn isotopes are included.

From the observed α energies and half lives of ^{194}At and ^{195}At, their α hindrance factors were calculated using a code in Ref. 57, assuming ground state transitions. Since the electron capture branches were not directly obtainable from our experiments due to the interferences from the directly produced proton-out products, they were assumed to be 10 percent according to Ref. 58. The results were 3.1 for ^{194}At and 2.4 for ^{195}At indicating both are allowed transition. To estimate the isotopes which the microsecond capability of the equipment allows us to study from the half life consideration alone, the partial α half lives of further neutron deficient At and Rn isotopes were calculated with the code used above together with the Q_α values obtained from the mass prediction by Liran and Zeldes. The ground state transitions were assumed in the calculations, and the α hindrance factor for each element was assumed to remain relatively constant as observed for their known neutron deficient isotopes. The representative values used (2.3 for At and 1.5 for Rn) were obtained by taking the average values of the four lightest known isotopes of each element. The result shown in Fig. 20 indicates the potential α identification capability of SASSY down to A=188 for At and A=190 for Rn considering only their α half lives.

While electron capture becomes an increasingly improbable mode of decay and becomes practically negligible for these isotopes, proton decay becomes conceivable for odd Z nuclei of At. Although precise proton half life prediction in this region is not possible at present due to the lack of data concerning the proton decay of relatively high Z elements, certain amounts of information can be extracted from the analogy carried over from the extensively studied α decay theory and its systematics. In particular, Nitschke obtained a semi-

empirical proton half life formula [59] equivalent to the Taagepera Nurmia formula for α decay [60], using the available proton decay data of lanthanide elements. Using this expression, assuming $J_p^{\pi}=\frac{5^+}{2}$, the partial proton half lives of At were estimated (Fig. 20). Notice the extremely fast decrease in the proton half life as the reduction of A, one may realize that even for the wide detection time range of our system, ^{188}At and ^{189}At are the only candidates whose proton decay mode may possibly be observed.

Probably the most severe limitation we will encounter comes from the low production cross section of these highly unstable nuclides. Thus it will be absolutely necessary to search for the best target-projectile combination for each nuclide to be produced. To find a suitable code for the production cross section, the excitation function for ^{56}Fe + ^{141}Pr was constructed (Fig. 21). The neutron evaporation code JORPLE, although it reinforced the validity of the assignments for ^{194}At and ^{195}At by correctly providing the optimum projectile energies for xn out products within 3 MeV (252 MeV for ^{194}At and 243 MeV for ^{195}At), failed to reproduce the excitation function for this reaction, which involves a large amount of charged-particle out products. The particle evaporation code ALICE [61], on the other hand, has been found to reproduce the observed excitation function reasonably well if the values in the Woods-Saxon (r_0,d) parameter space are fitted to the observation (Fig. 22). The best parameter values (r_0=1.23 fm, d=0.75 fm) were found for the excitation functions of ^{58}Fe+^{141}Pr, ^{56}Fe+^{142}Ce, ^{84}Kr+^{118}Sn, ^{72}Ge+^{127}I and ^{58}Fe+^{146}Nd, all yield compound nuclei in the same vicinity for Po, At and Rn. Care has to be taken, however, when we extrapolate more than 3 Z away from At, since we found these parameter values have to be readjusted rather drastically for the reactions which yield compound nuclei of Ra, Ac [46], largely due to the discrepancy in the estimate of not well known fission competition in this region. Using ALICE and these

parameter values, the excitation functions which yield the future candidates, ^{193}At, ^{197}Rn and ^{198}Rn as reaction products were constructed from all conceivable target-projectile combinations. For experimental feasibility, we restricted targets and projectiles to those that are stable and whose natural abundances exceed 1 and 5 percent respectively, and the reaction Q values obtained from the mass prediction by Liran and Zeldes were used in the calculation. The results are summarized in Fig. 23 for ^{193}At and in Fig. 24 for ^{197}Rn and ^{198}Rn. The peak cross sections for these isotopes in each reaction are plotted according to the projectile Z. It can be seen that reactions which involve exceptionally neutron-deficient targets like ^{144}Sm are definitely the most attractive candidates.

B. The evaluation of the equipment

It will be profitable to briefly review the characteristics of the equipment and to point out some of the most needed areas of improvement. The μsecond detection speed virtually eliminates the concern about the half life of nuclides to be produced in the near future, and probably this is all that is required for the detection of nuclides in the vicinity of At down to a few neutrons beyond the proton drip line as far as their α half lives are concerned. Although the ion optical transmission efficiency of 35 percent goes down to a final 10 percent for α detection when the geometry of α detectors and their 2π nature are considered, the employment of the α-α time-correlation technique, which can be applied more effectively for the short lived nuclides, will reduce the number of events necessary to a few at most to make an isotopic assignment. Although we observed a better than 10^{12} rejection factor against the full energy projectiles in this experiment, this value can be improved further by several orders of magnitude if necessary by the insertion of a stripper foil and a set of collimators in the dipole magnet. As a summary, the characteristic of our separator is

compared to that of the highly successful SHIP velocity filter at GSI in Table 1 [8]. It can be seen that the performances are quite comparable in spite of their gross differences in construction and principles of operation.

The most needed and effective improvement we can make is in the α detector array itself. The equipment described in this work often did not have the capability to successfully correlate a mother-daughter α pair separated more than 20 sec due to interference from the directly produced daughter-like products which traversed through the separator unrejected. Conversion to a position-sensitive detector array will virtually eliminate this problem and extend the usable correlation time to the order of an hour. The improvement of α energy resolution will be another significant addition. This is because the neutron deficient isotopes, which lie below the 126 neutron shell, have been observed to possess isomeric states (Fig. 17). In the vicinity of At, these states are assigned $I^{\pi}=\frac{13^{+}}{2}$ for the odd mass Po and Pb isotopes, and $I^{\pi}=10^{-}$ for the even mass Bi isotopes [4]. Realizing that these high spin states tend to be populated rather intensely by the heavy ion reactions such as the one employed in this work [62], the possibility that the α activities assigned for the At isotopes can not be excluded as being a mixture of closely spaced ground and isomeric transition. The present detectors, which are designed for maximum efficiency, simply do not meet the energy resolution requirements for the isomeric transition which often produces counterparts as close as 50 KeV to its ground state, and detector modifications along this line are desired to be undertaken [40].

C. The hopes for future extension of nuclides in this vicinity

We considered a few prospective methods to produce more neutron-deficient nuclides in this vicinity. If we stay close to reactions like Fe+Pr,

where we have gained some experience, probably the first attempt should be to use a highly neutron-deficient target like ^{144}Sm with some appropriate projectiles. This combination should produce a somewhat more neutron-deficient compound nucleus with comparable excitation energy to that of Fe+Pr. Secondly the use of neutron-deficient projectiles such as ^{54}Fe from the unenriched ion source, for example, can be considered seriously when we recall the improved capability of the new injector installed at the SuperHILAC. Thirdly if we prefer to take a somewhat more adventurous route, we can always depart from reactions like Fe+Pr altogether and try something different. One such attempt comes from the recognition of the other minima appearing at the excitation energy illustrated in Fig. 7. This often neglected minimum which is associated with more symmetric target-projectile combinations, deserves more attention, since highly neutron-deficient systems can be reached (Fig. 25) [63,64]. The somewhat suppressed cross section of 0.2 μbarn for ^{194}At observed in the cross bombardment ^{84}Kr+^{113}In might be attributed to the extra projectile energy presumably needed for heavy less asymmetric reactions [51,65]. Although this may tend to discourage us to use these reactions extensively in the immediate future until the conventional reactions are all exhausted, one may realize that these are the only realistic reactions which may lead to the production of ultimately neutron-deficient proton emitters in this region. The production of nuclides in this vicinity by symmetric as well as asymmetric combinations is currently under investigation [66] and we hope these reactions will extend the boundary of existing nuclides and bring us a deeper understanding of these highly unstable nuclides which appear far off the stability line.

REFERENCES

(1) E. Curie, Madame Curie, a biography, (Doubleday & Doran, New York, 1938).

(2) Nuclear Chemistry, edited by G. T. Seaborg and W. Loveland (Hutchinson Ross, Pennsylvania, 1982).

(3) E. K. Hyde, I. Perlman and G. T. Seaborg, The nuclear properties of the heavy elements, (Dover, New York, 1964).

(4) Table of Isotopes, 7th ed., edited by C. M. Lederer and V. S. Shirley (Wiley, New York, 1978).

(5) D. Scott, LBL-7111 (1977).

(6) G. Rudstam Proc. of the Int'l symp. on nuclides far off the stability line, Lysekil Sweden, Aug. 21-27, 1966; (Almqvist and Wiksell, Stockholm) P. 9.

(7) High Intensity Uranium Beams. National Facility from the superHILAC and BEVALAC, Technical Description, Lawrence Berkeley Laboratory, Feb. 1979, PUB. 5023.

(8) G. Münzenberg, W. Faust, S. Hofmann, P. Armbruster, K. Güttner, and H. Ewald, Nucl. Instr. and Meth. 161, 65 (1979).

(9) Proc. of the 10th Int'l Conf on Electromagnetic isotope separators and techniques related to their applications, Zinal, Switzerland, Sep. 1-6, 1980 edited by E. Kugler and S. Sundell (North Holland, Amsterdam, 1981).

(10) M. E. Leino, S. Yashita and A. Ghiorso, Phys. Rev. C24, 2370 (1981).

(11) S. Yashita, M. E. Leino and A. Ghiorso, LBL-11588, p. 88.

(12) P. Marmier and E. Sheldon, Physics of Nuclei and Particles, Vol. 1, (Academic press, New York, 1969) p. 612.

(13) P. Armbruster, Proc. of the 3rd Int'l Conf on Nuclei far from Stability, Cargese, Corsica, Mar. 19-26, 1976.

(14) A. C. Paul, LBL-2697 (1975). (BELIN is a version of TRANSPORT described in this report.)

(15) see p. 698 of (12) or p.123 of (33).

(16) C. B. Fulmer and B. L. Cohen, Phys. Rev. 109, 94 (1958).

(17) B. L. Cohen and C. B. Fulmer, Nucl. Phys. 6, 547 (1958).

(18) Methods of Experimental Physics, Vol. 17, edited by P. Richard (Academic press, New York, 1980) p.129.

(19) P. Armbruster, J. Eidens, J. W. Gruter, H. Lawin, E. Roeckl, and K. Sistemich, Nucl. Instr. and Meth. 91, 499 (1971).

(20) H. Lawin, J. Eidens, P. Armbruster, J. W. Gruter, K. Hubenthal, and K. Sistemich, Proc. Int. Conf. on Electromagnetic isotope separators and the techniques of their applications, Marburg 1970, edited by H. Wagner and W. Walcher, p. 270.

(21) H. H. Heckman, E. L. Hubbard, and W. G. Simon, Phys. Rev. 129, 1240 (1963).

(22) H. D. Betz, Rev. Mod. Phys. Vol. 44, no.3, 465 (1972).

(23) V. S. Nikolaev, and I. S. Dimitriev, Phys. Lett. 28A, 277 (1968).

(24) V. A. Karnaukhov, L. Rubinskaya, G. M. Ter Akop'Yan, V. Titov, and V. A. Chugreev, JINR p13-4454 (Dubna 1969).

(25) I. Bacho, D. D. Bogdanov, S. Daroczy, V. A. Karnaukhov, L. A. Petrov, and G. M. Ter Akop'Yan, JINR p13-4453 (1969).

(26) L. A. Petrov, V. A. Karnaukhov, and D. D. Bogdanov, JINR p7-5180.

(27) L. Meyer, Phys. Stat. sol. (B) 44, 253 (1971).

(28) R. D. Cowan, Rhys. Rev. 163, 54 (1967).

(29) R. D. Cowan and D. C. Griffin, J. Op. Soc. Am. 66, 1010 (1976).

(30) A. Ghiorso, M. E. Leino, S. Yashita, L. Frank, P. Armbruster, J. P. Dufour and P. K. Lemmertz, LBL-15955 (1983).

(31) H. Stelzer and A. Baden, GSI report 81-2, ISSN0174-0814 (1981) p.203.

(32) G. F. Knoll, Radiation Detection and Measurement, (wiley, New York, 1979) p.141.

(33) E. Segre, Nuclei and Particles, 2nd ed., (Benjamin/Cummings, Reading, 1977) p. 122.

(34) G. G. Eichholz, and J. W. Poston, Principles of Nuclear Radiation Detection, (Ann Arbor Science, Ann Arbor, 1979).

(35) W. D. Myers, Droplet model of atomic nuclei, (IFI/Plenum, 1977).

(36) K. H. Schmidt, W. Faust, G. Münzenberg, H. G. Clerc, W. Lang, K. Pielenz, D. Vermeulen, H. Wohlfarth, H. Ewald, and K. Güttner, Nuclear Physics A318, 253, (1979).

(37) F. P. Heβberger, s. Hofmann, G. Münzenberg, W. Reisdorf, J. R. H. Schneider, and P. Armbruster, GSI Annual Report 1982.

(38) S. Hofmann, G. Münzenberg, F. Heβberger, W. Reisdorf, P. Armbruster, and B. Thuma Z. Phys. A299, 281 (1981).

(39) S. Hofmann, W. Faust, G. Münzenberg, W. Reisdorf, P. Armbruster, K. Güttner, H. Ewald, Z. Physik A291, 53 (1979).

(40) A. Ghiorso, M. E. Leino, S. Yashita, P. Armbruster, J. P. Dufour, S. Hofmann, P. Lemmertz and G. Münzenberg, GSI Annual Report (1982).

(41) G. Münzenberg, S. Hofmann, F. P. Heβberger, W. Reisdorf, K. H. Schmidt, J. H. R. Schneider, P. Armbruster, C. C. Sahm, and B. Thuma, Z. Physik., A300, 107 (1981).

(42) G. Münzenberg, P. Armbruster, F. P. Heβberger, S. Hofmann, K. Poppensieker, W. Reisdorf, J. H. R. Schneider, K. -H. Schmidt, C. -C. Sahm and D.

Vermeulen, Z. Physik., A309, 89 (1982).

(43) W. Treytl and K. Valli, Nuclear Physics A97, 405 (1967).

(44) Yu. Ts. Organessian, JINR d7-8194 (1974).

(45) P. Armbruster, "Cold Rearrangement of Nucleons in Fission and Fusion." GSI 1982-5, preprint.

(46) J. R. Alonso, C. T. Alonso, A. Ghiorso, J. M. Nitschke, and M. Nurmia, LBL annual report 1974, LBL- 4000, p.47.

(47) Y. LeBeyec, R. L. Hahn, K. S. Toth, and R. Eppley, Phys. Rev. C14, 1038, (1976).

(48) K. E. Williams, LBL-7714 (1978).

(49) J. Blocki, J. Randrup, W. J. Swiatecki and C. F. Tsang, LBL-5014 (1976).

(50) J. Randrup, LBL-5847 (1976).

(51) S. Bjornholm and W. J. Swiatecki, LBL-14074, (1982).

(52) Handbook of Chemistry and Physics, 46th edition, B-129 (Chemical Rubber Co. 1964).

(53) J. Alonso, Gmelins Handbuch der anorganischen Chemie, Ergänzungswerk (Springer, Berlin, 1974), Vol. 7b, A1, II.

(54) A. S. Green, Rev. Mod. Phys., 30, 569 (1958).

(55) R. C. Eggers and L. P. Somerville, Nucl. Instr. and Meth. 190, p.535 (1981).

(56) S. Maripuu, At. Data Nucl. Data Tables, 17, 476 (1976).

(57) H. V. Michel, UCRL-9229 (1960).

(58) K. Takahashi, M. Yamada and T. Kondoh, At. Data Nucl. Data. Tables, 12, 101 (1973).

(59) J. M. Nitschke, to be published in LBL nuclear science annual report (1983).

(60) R. Taagepera and M. Nurmia, Ann. Acad. Sci. Fenn. Ser. A, Sec. VI, No. 78 (1961).

(61) M. Blann and J. Bisplinghoff, UCID-19614 (1982).

(62) T. Sikkeland, R. J. Silva, A. Ghiorso and M. J. Nurmia, Phys. Rev. C1, 1564 (1970).

(63) H. Gauvin, Y. Le Beyec, M. Lefort, and C. Deprun, Phys. Rev. Lett. 28, 697 (1972).

(64) R. Hingmann, H. G. Clerc, C. C. Sahm, and D. Vermeulen, GSI annual report 1982, 65.

(65) W. J. Swiatecki, LBL-12642, (1981).

(66) M. E. Leino, K. Moody, S. Yashita and A. Ghiorso, LBL-15563 (1983).

FIGURE CAPTIONS

(1) SASSY over all view.

(2) The BELIN plot indicating the focusing characteristics of SASSY.

(3) The dependence of the magnetic rigidity on Z. The dashed curve indicates the prediction by Eq. 1c. The prediction according to the Bohr-Lamb criteria is shown as the solid serrated line.

(4) Arrangement of electronic detectors used for the experiment.

(5) Block diagram of the electronics.

(6) The dependence of the fission barrier (solid line) and the proton binding energy (dashed line) on the most neutron deficient known isotopes of element, Z.

(7) The excitation energy of ^{197}At in various target-projectile combinations from Ref. 34, 48 and 49 (dashed line). The one which includes the extra energy [60] is shown by a solid line.

(8) Time-of-flight spectra taken at E_{Lab}=255MeV.

(9) The two dimensional density plot of time-of-flight against recoil energy. E_{Lab}=255 MeV.

(10) The recoil energy spectra at the same projectile energy. The recoil events which are time-correlated with the ^{194}Po 6.84 MeV α after the subtraction of accidentals and those which are correlated with the newly discovered 7.20 MeV α together with the estimated accidentals are included in this figure.

(11) The α spectra taken at 255 MeV for the projectile energy.

(12) The decay curve for the 7.20 MeV activity assigned to ^{194}At.

(13) The α spectra of events which are time-correlated with the 7.20 MeV α within 10.0 sec. The estimated accidentals are shown by the solid curve.

(14) The α spectra taken at the projectile energy of 249 MeV.

(15) The α-α correlation for ^{195}At.

(16) The decay curve for the 7.12 MeV activity assigned to ^{195}At.

(17) The α systematics of neutron-deficient isotopes of Po, At, Rn and Fr.

(18) The α energies of neutron deficient At isotopes and their comparison to the ones estimated from several mass predictions in Ref. 56.

(19) Prediction of proton binding energies for the neutron deficient At isotopes.

(20) The partial α and proton half life predictions for At and Rn isotopes. The open symbols indicate the nuclides beyond the proton drip line.

(21) The excitation function for the reaction ^{58}Fe+^{141}Pr.

(22) The excitation function generated by the ALICE code. r_0=1.23 fm and d=0.75 fm were used for this calculation.

(23) The ^{193}At production cross section predicted by ALICE for various target-projectile combinations according to Z of the projectile. The corresponding targets are implied.

(24) The production cross section predictions for ^{197}Rn and ^{198}Rn.

(25) The most neutron deficient compound nuclides of At and Rn which can be reached, without difficulty, by various target-projectile combinations. The location of the next new isotopes are indicated.

	SHIP	SASSY
Acceptances		
Relative Charge	20%	100%
Relative Velocity	10%	40%
Angle	3°	3°
Halfwidth in focal plane	40 x 20 mm	50 x 20 mm
Beam Supression	10^{12} - 10^{17}	10^{15}
Transfer Supression	10^{4}	> 10^{3}
Experimental efficiency for Alpha-decays	20%	15%

Table 1: A comparison of the velocity filter SHIP and the gas-filled separator SASSY for fusion reactions. The data for both types of set ups are somewhat reaction dependent.

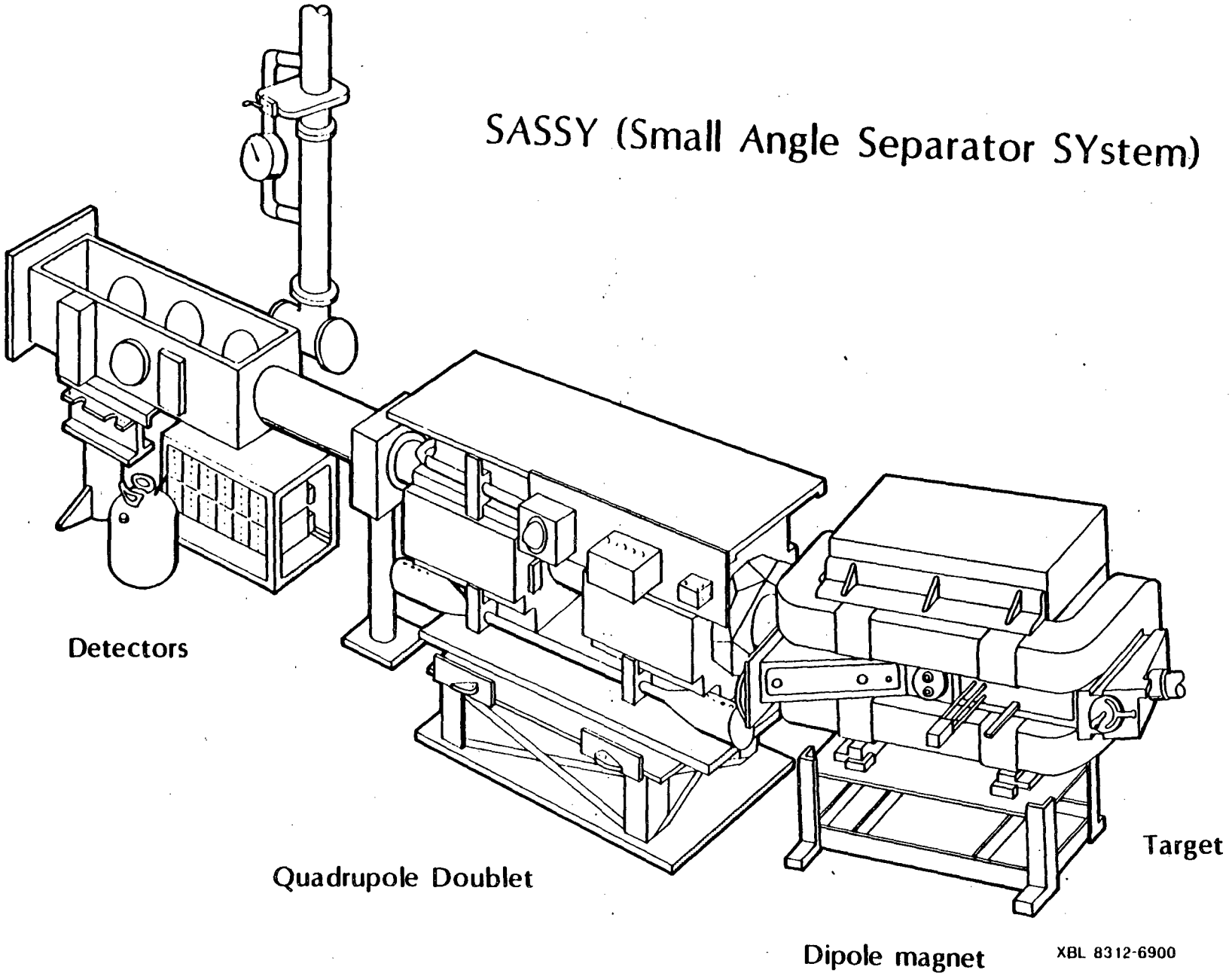
SASSY (Small Angle Separator SYstem)
Detectors
Quadrupole Doublet
Dipole magnet
Target
XBL 8312-6900

Fig. 1

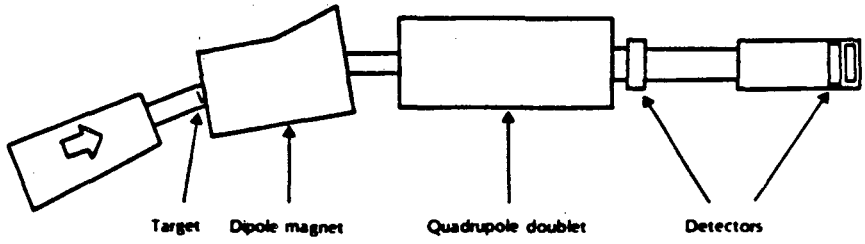
Target
Dipole magnet
Quadrupole doublet
Detectors

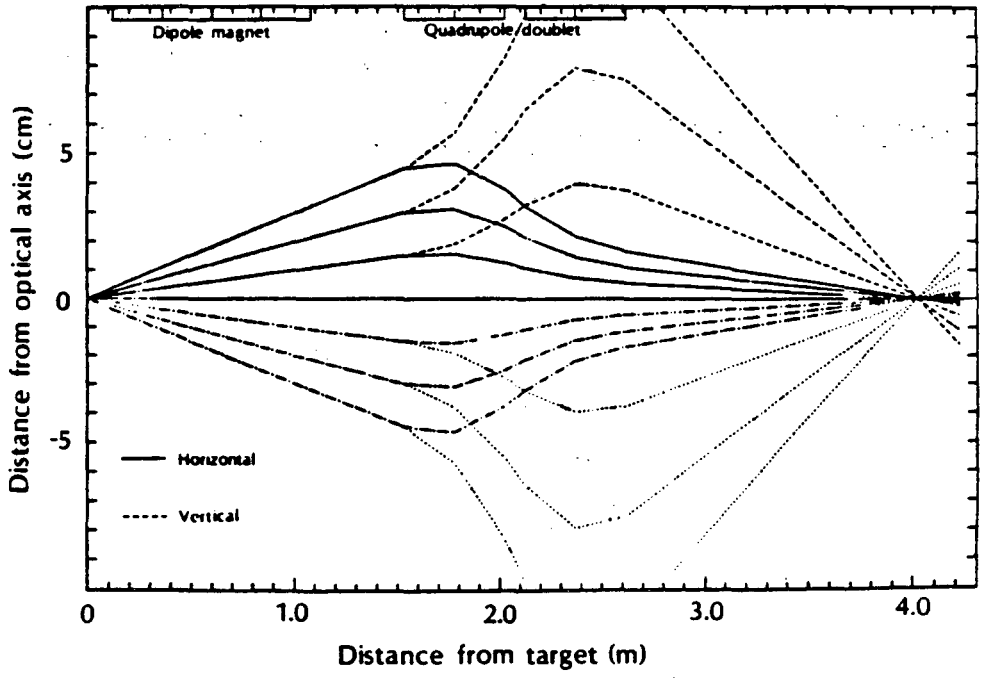
Dipole magnet
Quadrupole/doublet
Distance from optical axis (cm)
5
0
-5
Horizontal
Vertical
0
1.0
2.0
3.0
4.0
Distance from target (m)

Fig. 2

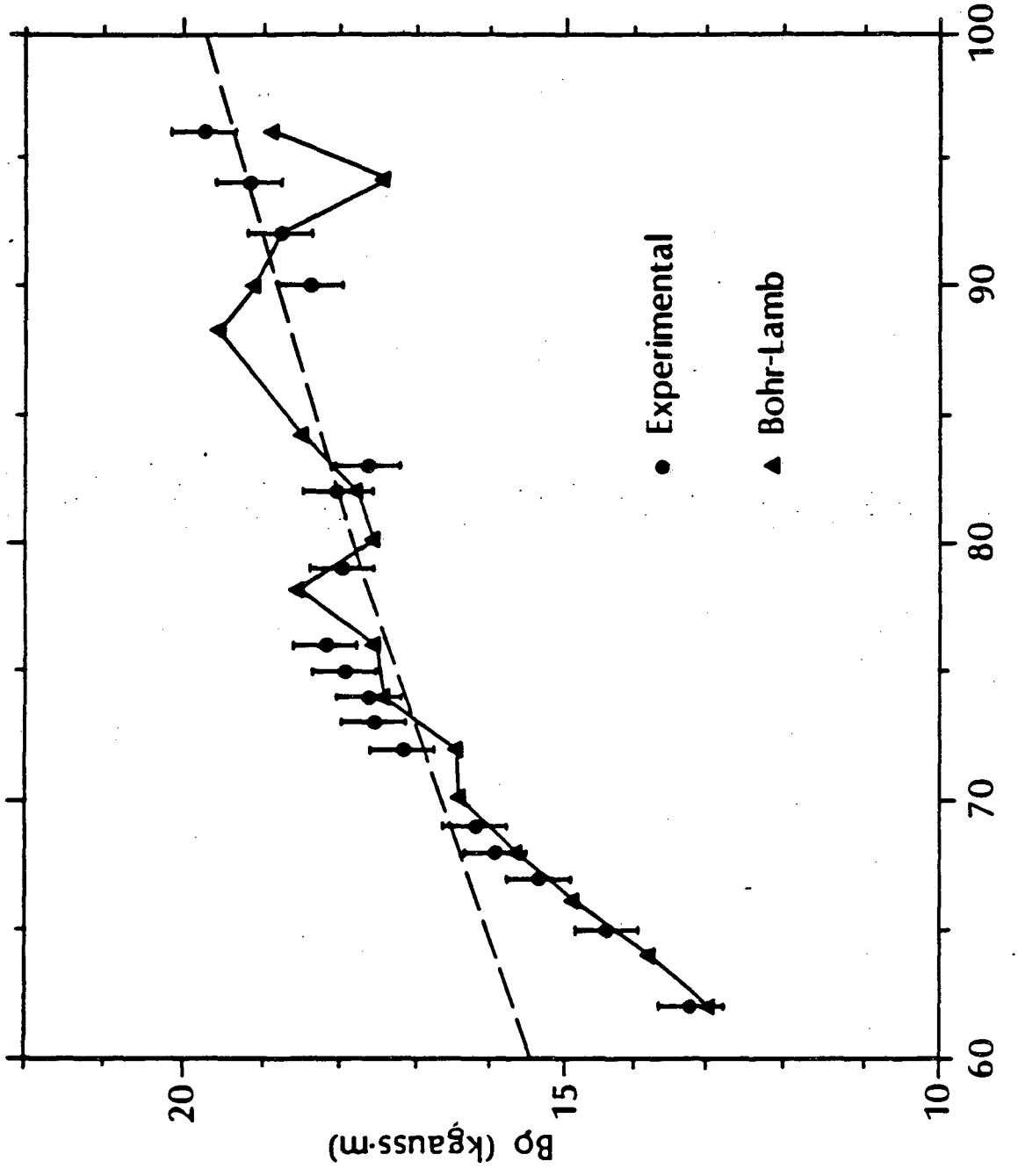

Fig. 3

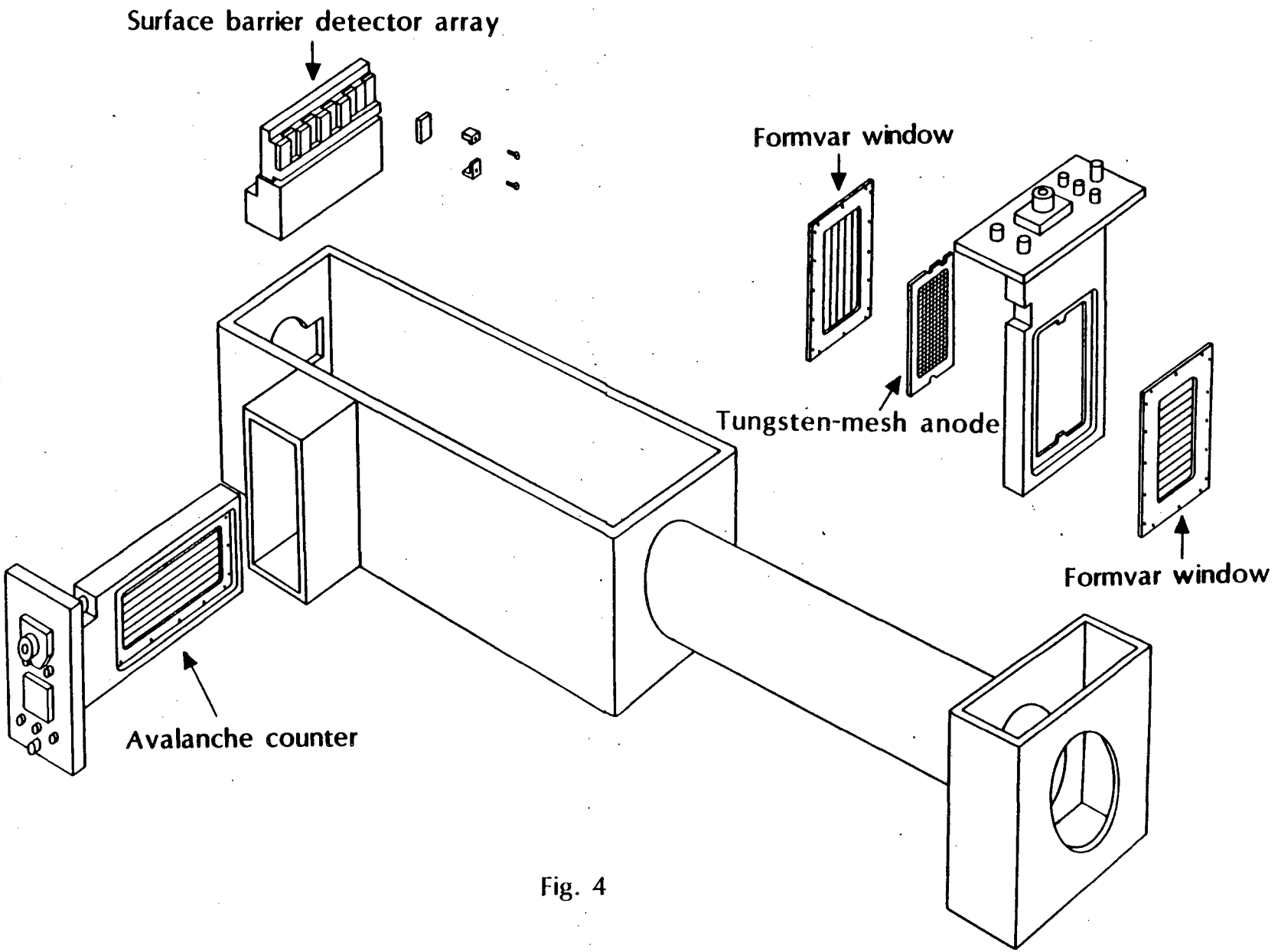
Surface barrier detector array
Formvar window
Tungsten-mesh anode
Formvar window
Avalanche counter

Fig. 4

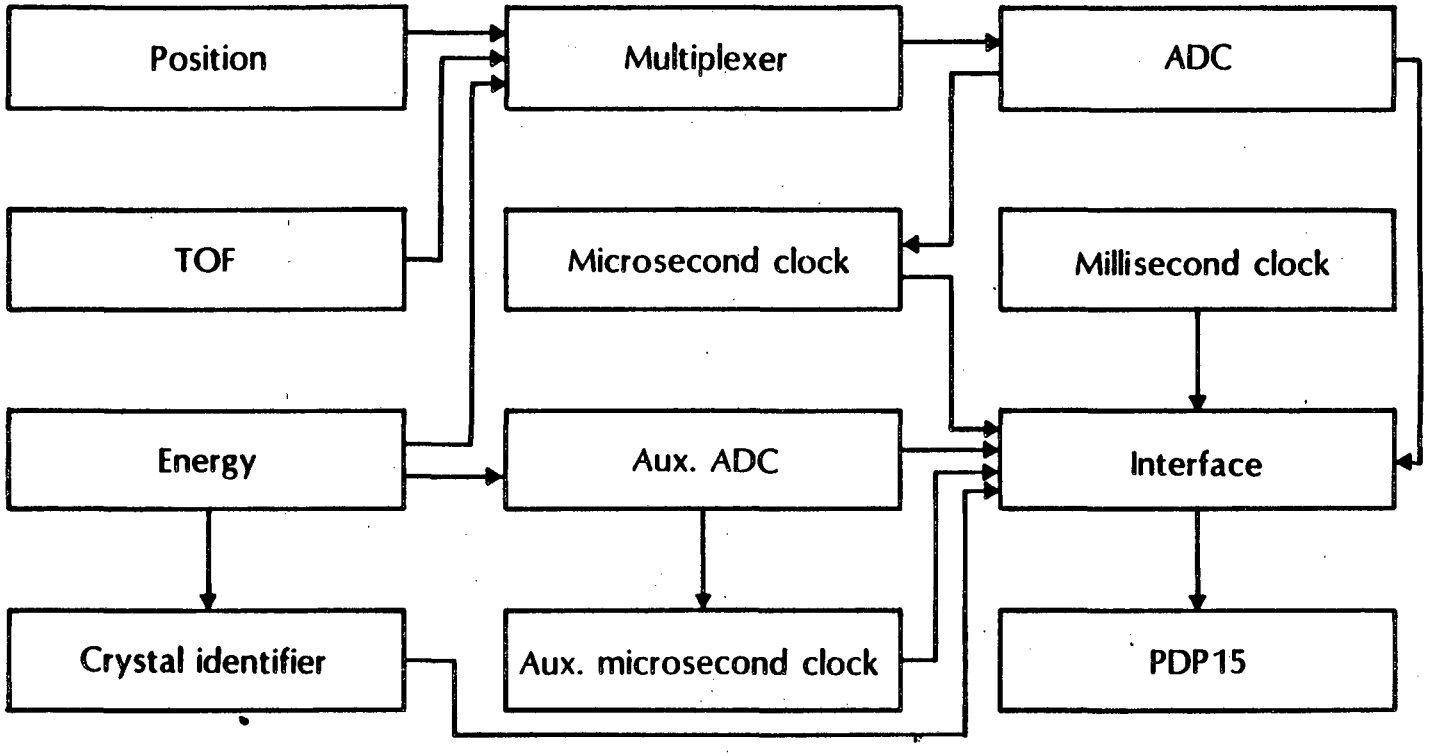
Position
Multiplexer
ADC
TOF
Microsecond clock
Millisecond clock
Energy
Aux. ADC
Interface
Crystal identifier
Aux. microsecond clock
PDP15

Fig. 5

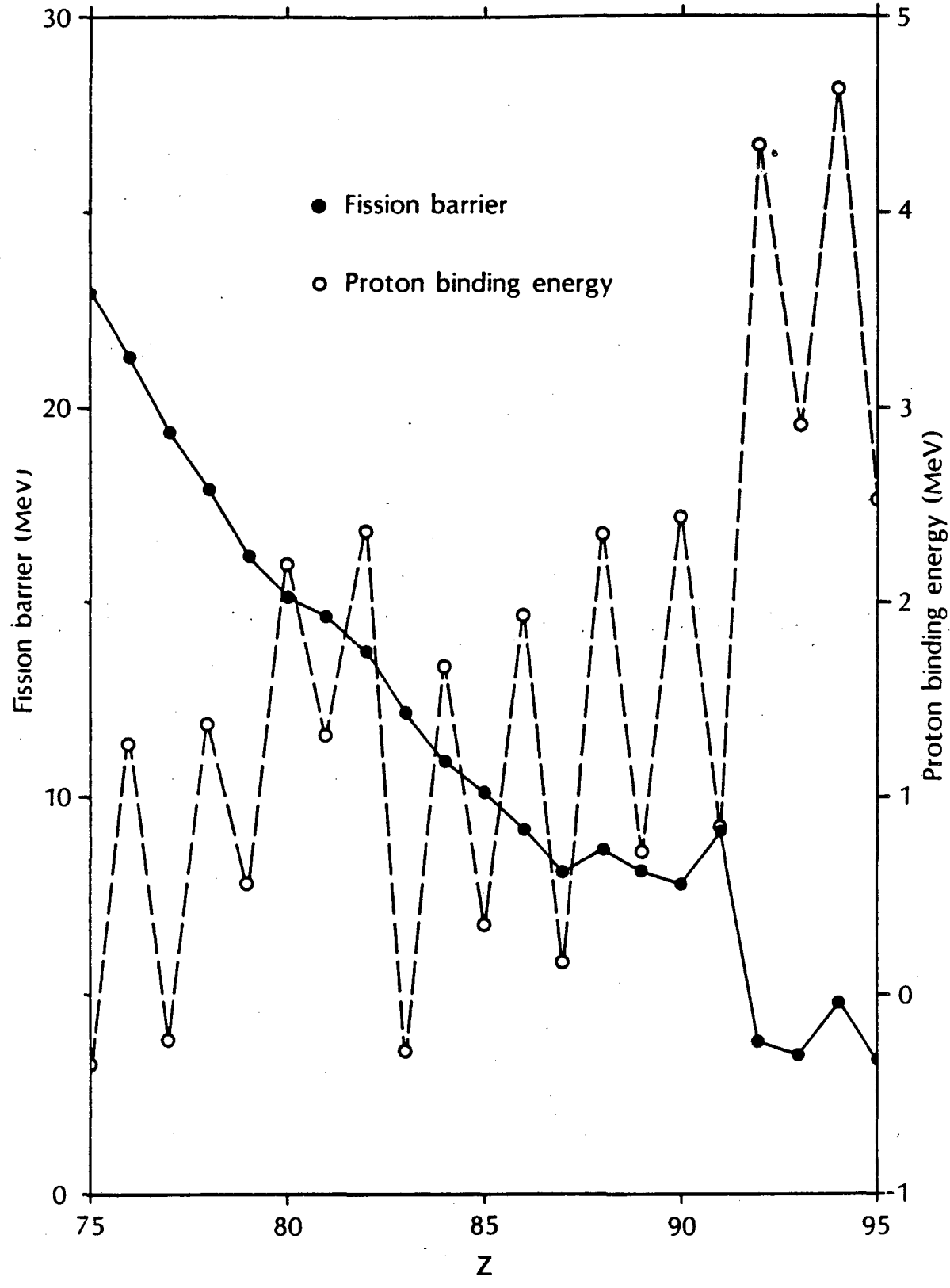
Fission barrier
Proton binding energy
Fission barrier (MeV)
Proton binding energy (MeV)
Z
30
20
10
0
5
4
3
2
1
0
-1
75
80
85
90
95

Fig. 6

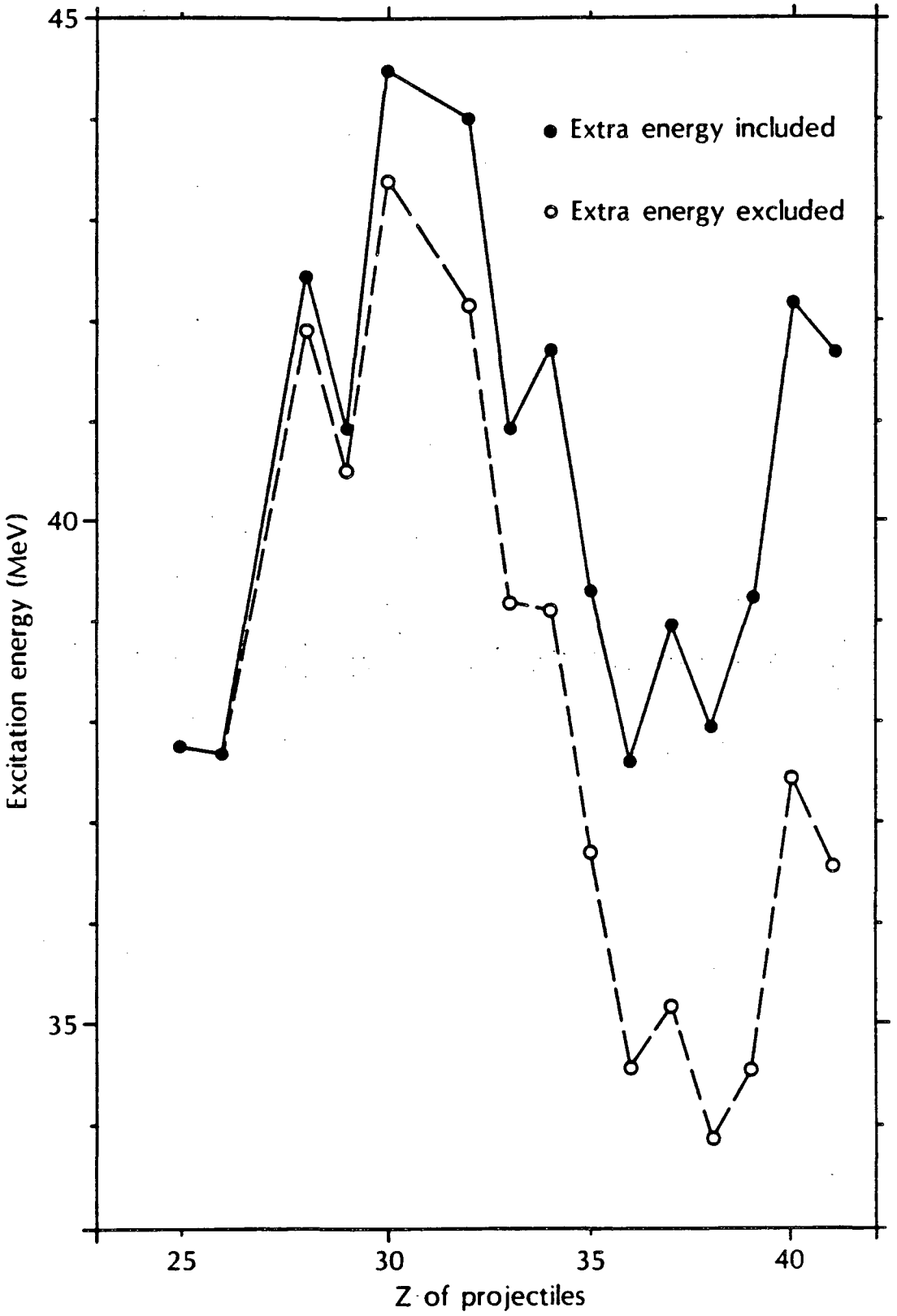
45
40
35
Excitation energy (MeV)
Extra energy included
Extra energy excluded
25
30
35
40
Z of projectiles

Fig. 7

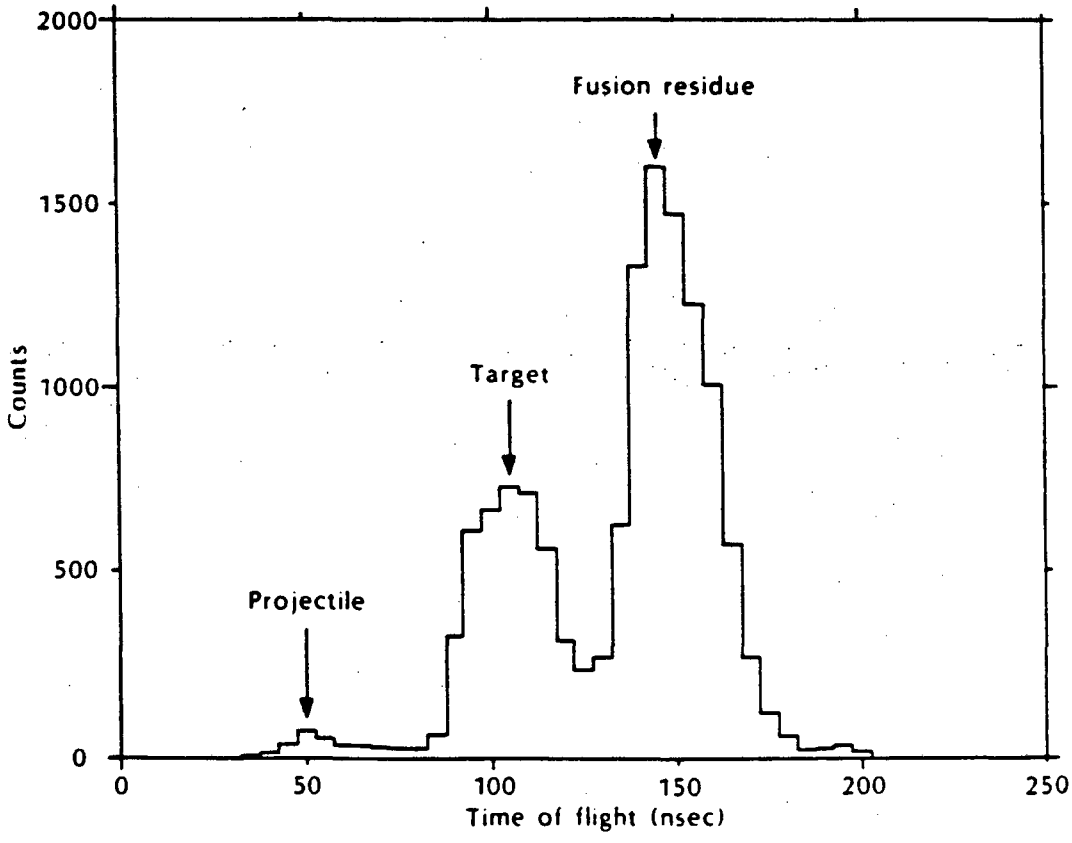
2000
1500
1000
500
0
Counts
Fusion residue
Target
Projectile
0
50
100
150
200
250
Time of flight (nsec)

Fig. 8

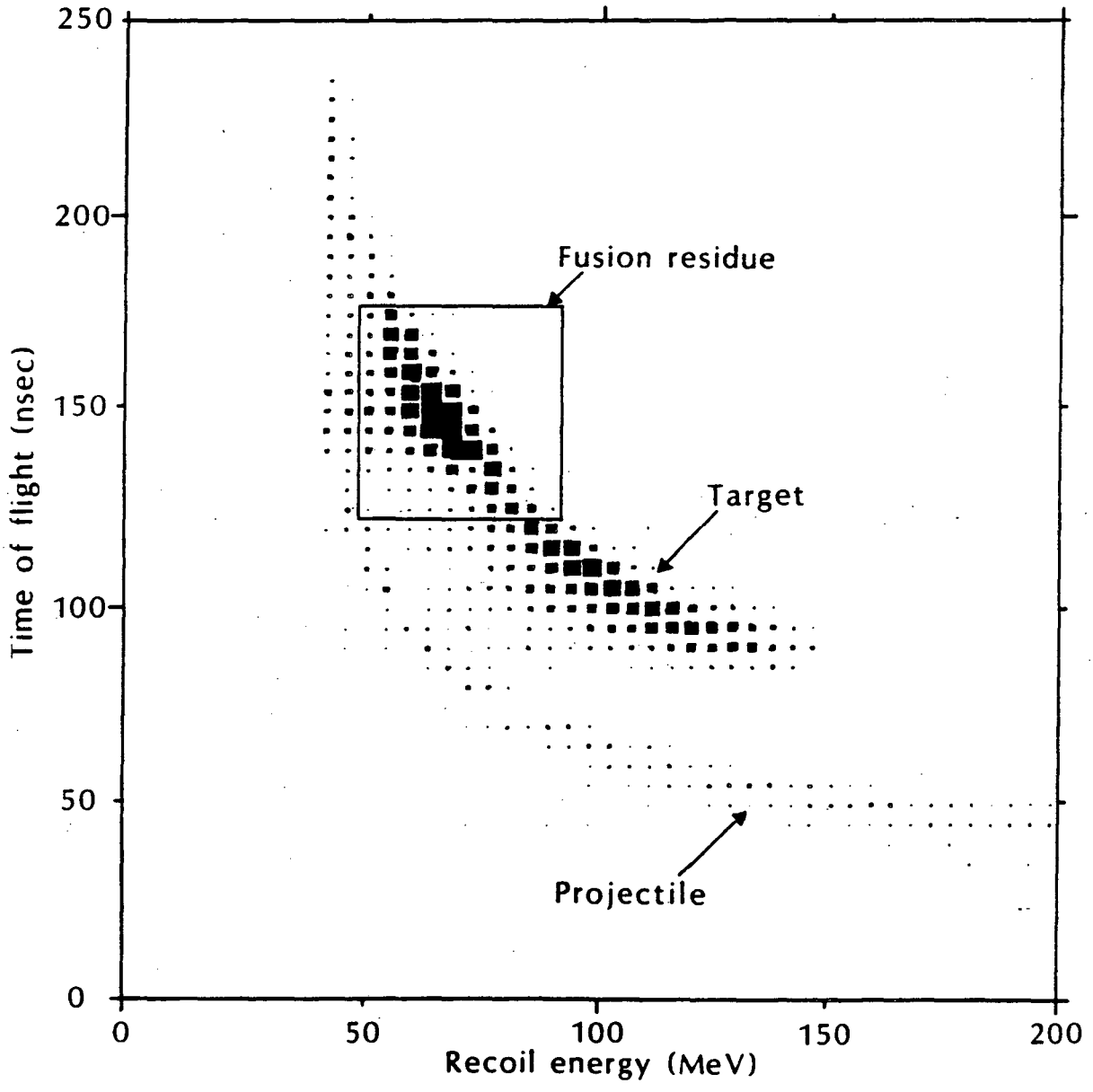
250
200
150
100
50
0
Time of flight (nsec)
Fusion residue
Target
Projectile
0
50
100
150
200
Recoil energy (MeV)

Fig. 9

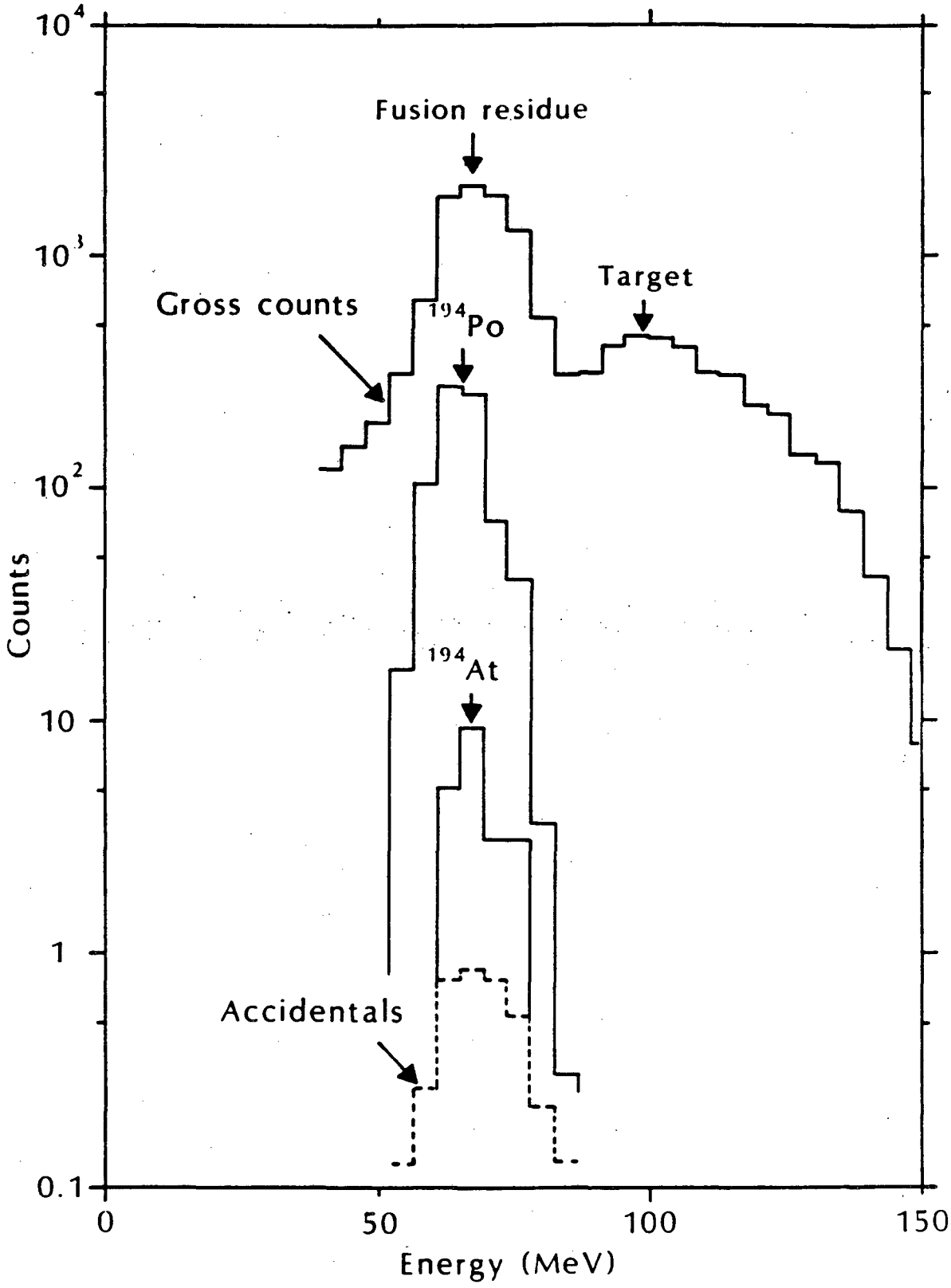
10^4
10^3
10^2
10
1
0.1
Counts
Fusion residue
Target
Gross counts
^{194}Po
^{194}At
Accidentals
0
50
100
150
Energy (MeV)

Fig. 10

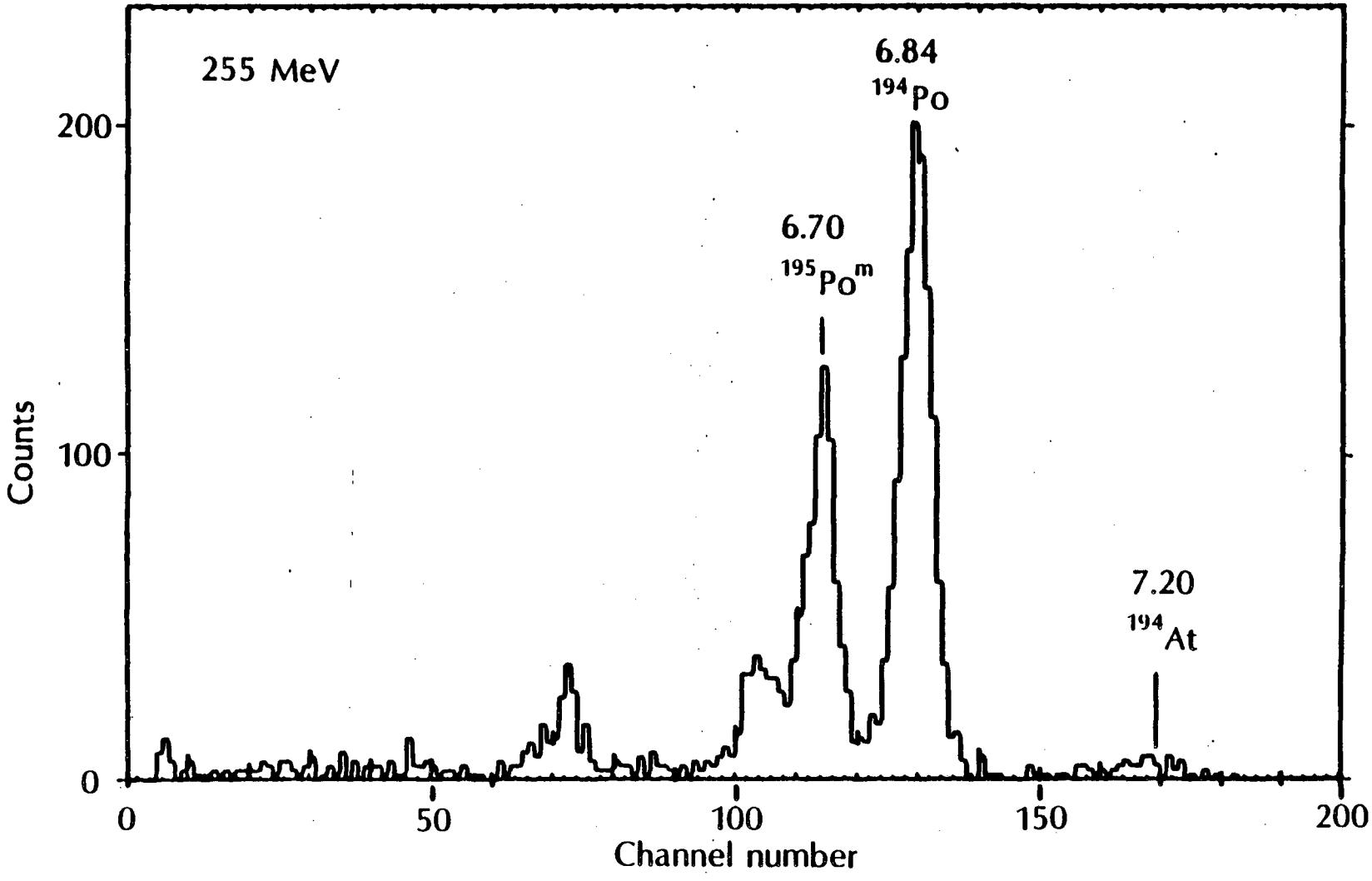
255 MeV
6.84
194Po
6.70
195Pom
7.20
194At
Counts
200
100
0
0
50
100
150
200
Channel number

Fig. 11

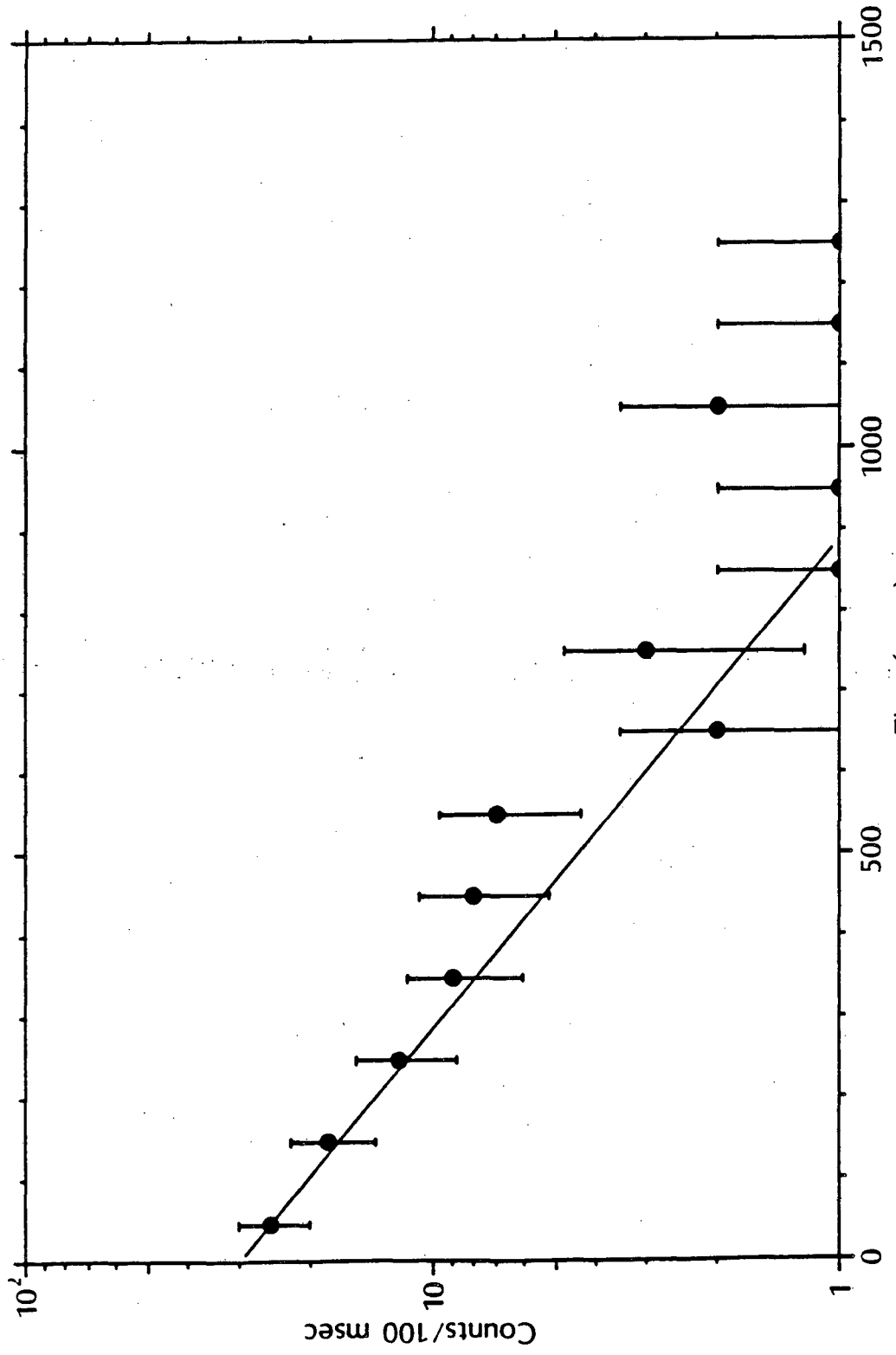

Fig. 12

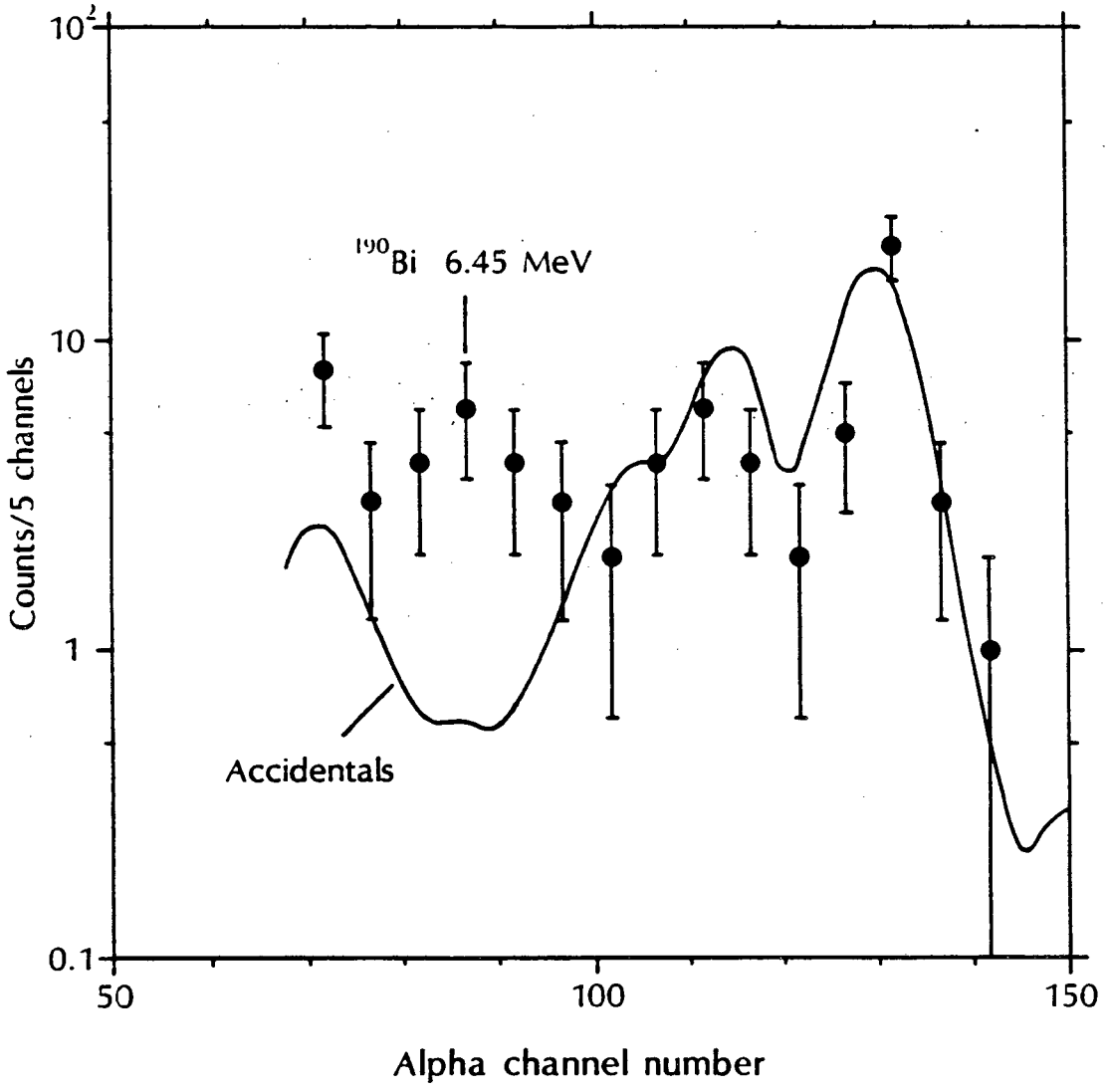
10^2
10
1
0.1
Counts/5 channels
^{190}Bi 6.45 MeV
Accidentals
50
100
150
Alpha channel number

Fig. 13

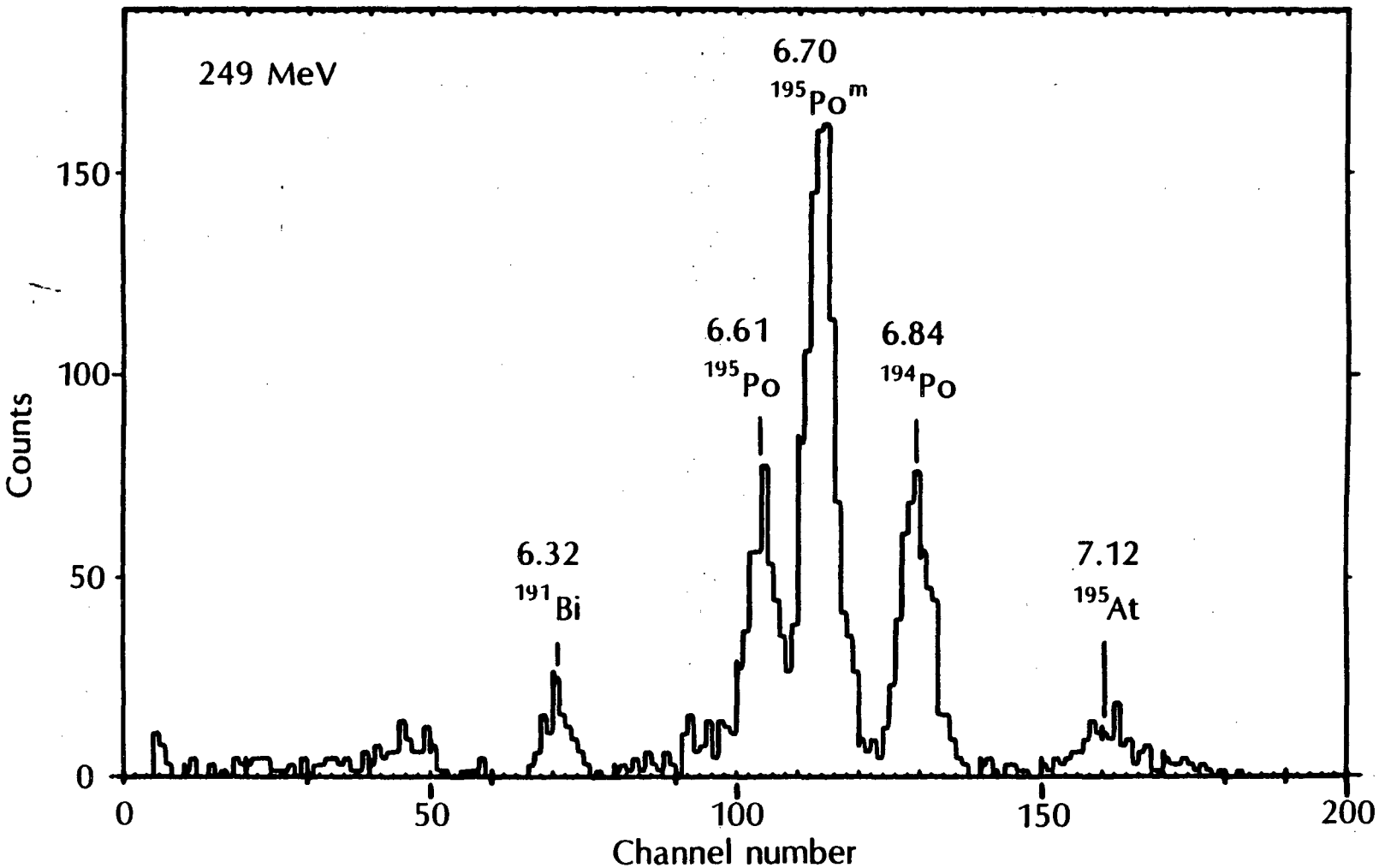
249 MeV
6.70
195Pom
6.61
195Po
6.84
194Po
6.32
191Bi
7.12
195At
Counts
Channel number
0
50
100
150
200

Fig. 14

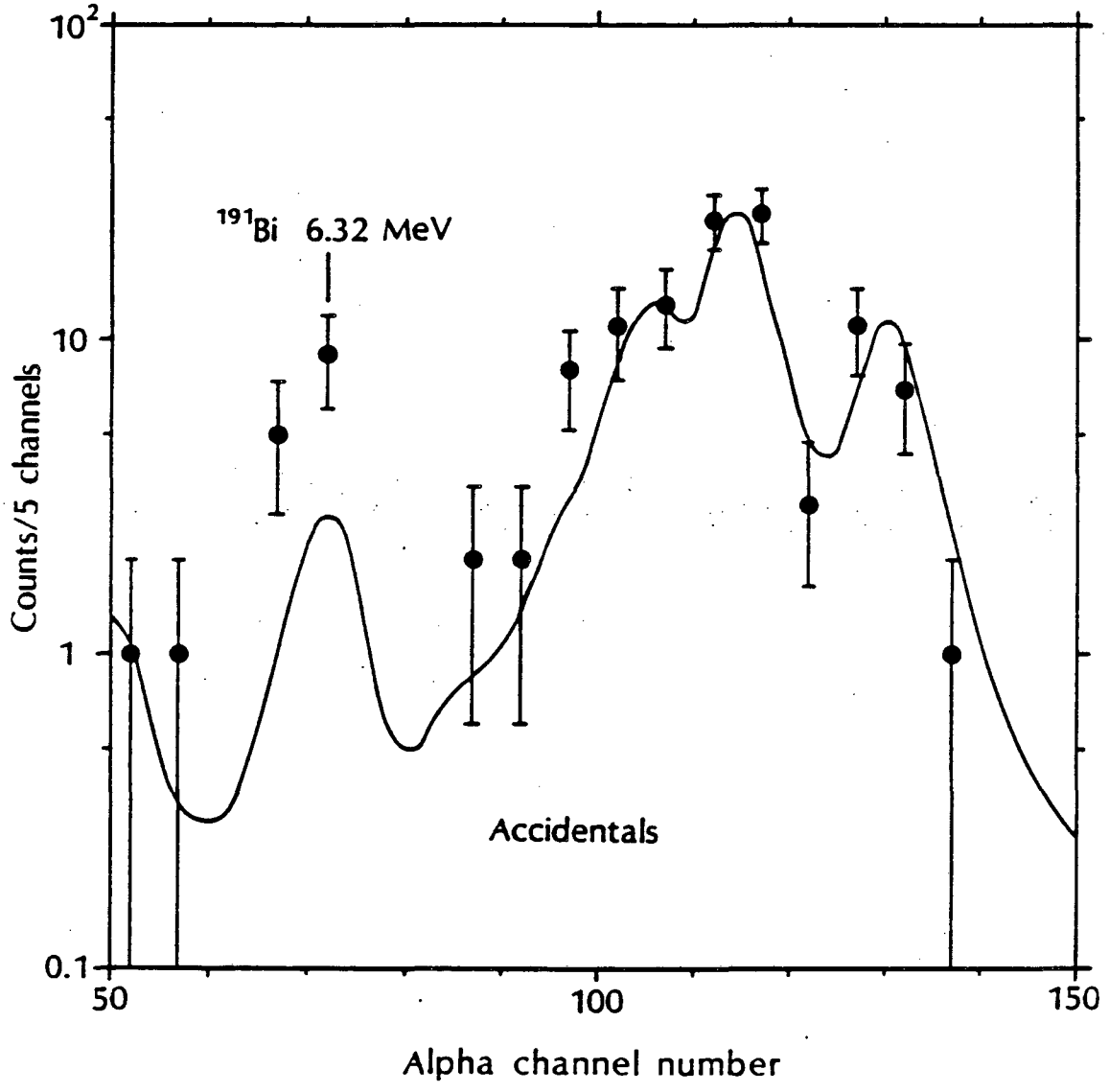
10^2
10
1
0.1
Counts/5 channels
^{191}Bi 6.32 MeV
Accidentals
50
100
150
Alpha channel number

Fig. 15

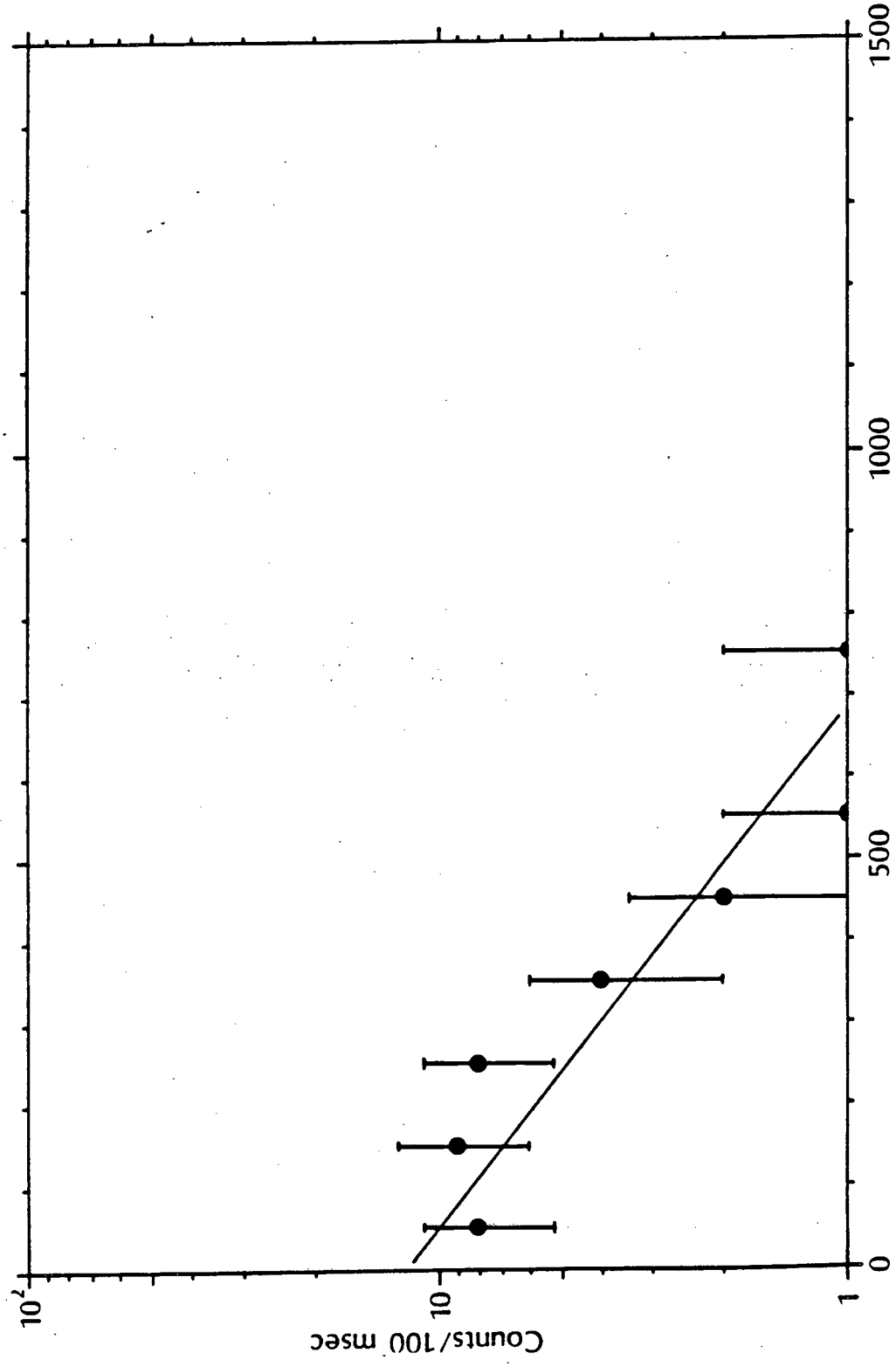

Fig. 16

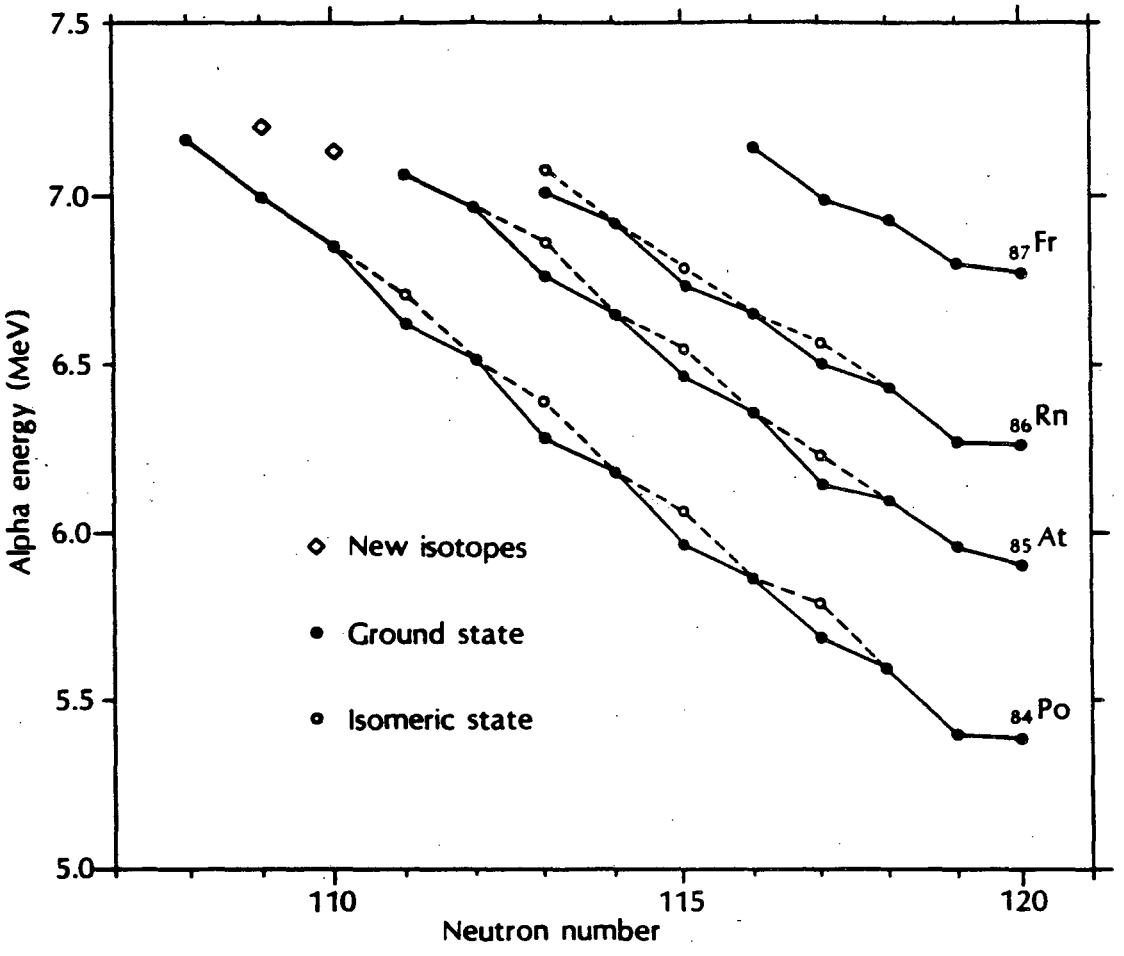
7.5
7.0
6.5
6.0
5.5
5.0
Alpha energy (MeV)
110
115
120
Neutron number
New isotopes
Ground state
Isomeric state
87Fr
86Rn
85At
84Po

Fig. 17

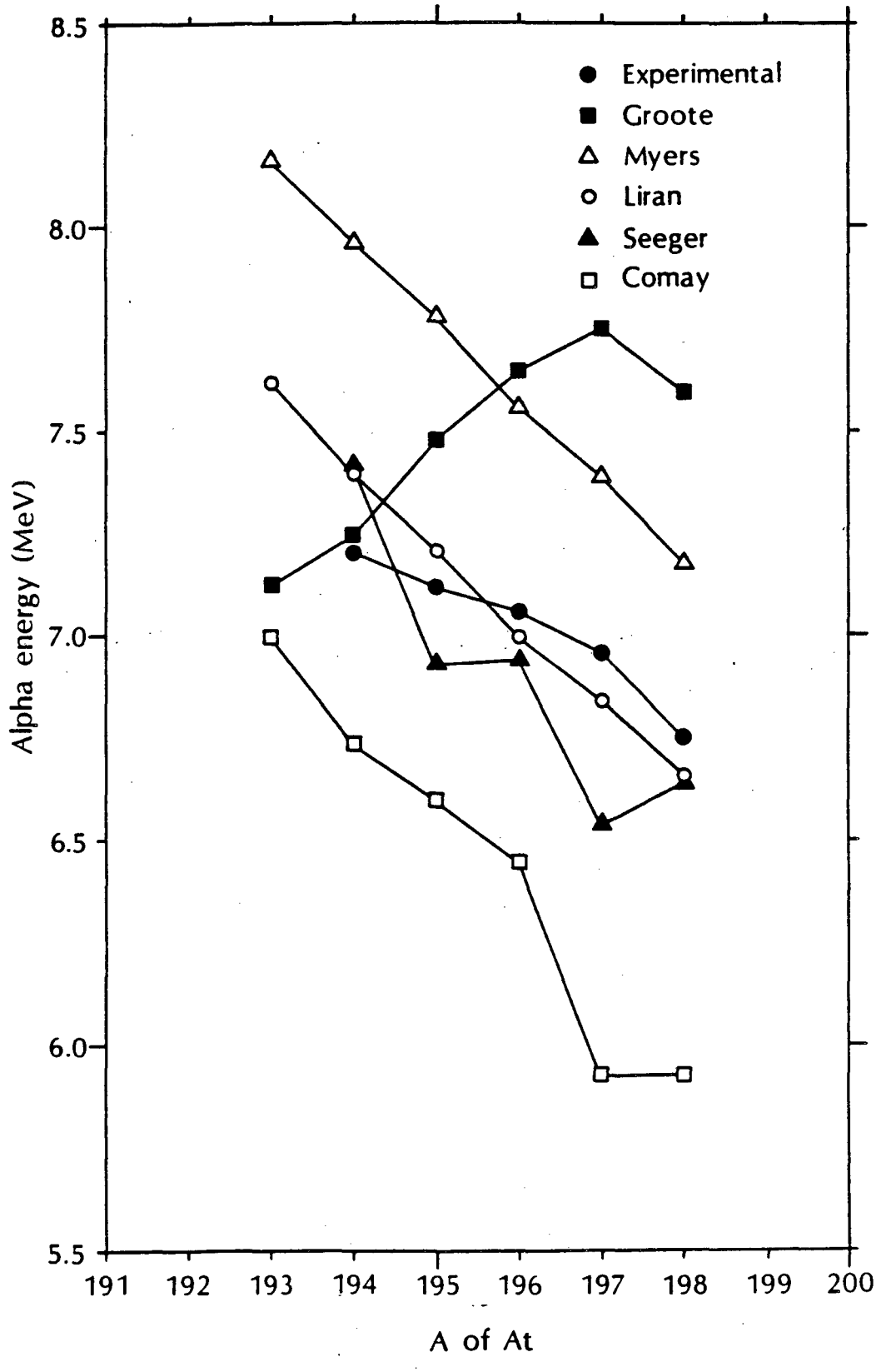
8.5
8.0
7.5
7.0
6.5
6.0
5.5
Alpha energy (MeV)
191
192
193
194
195
196
197
198
199
200
A of At
Experimental
Groote
Myers
Liran
Seeger
Comay

Fig. 18

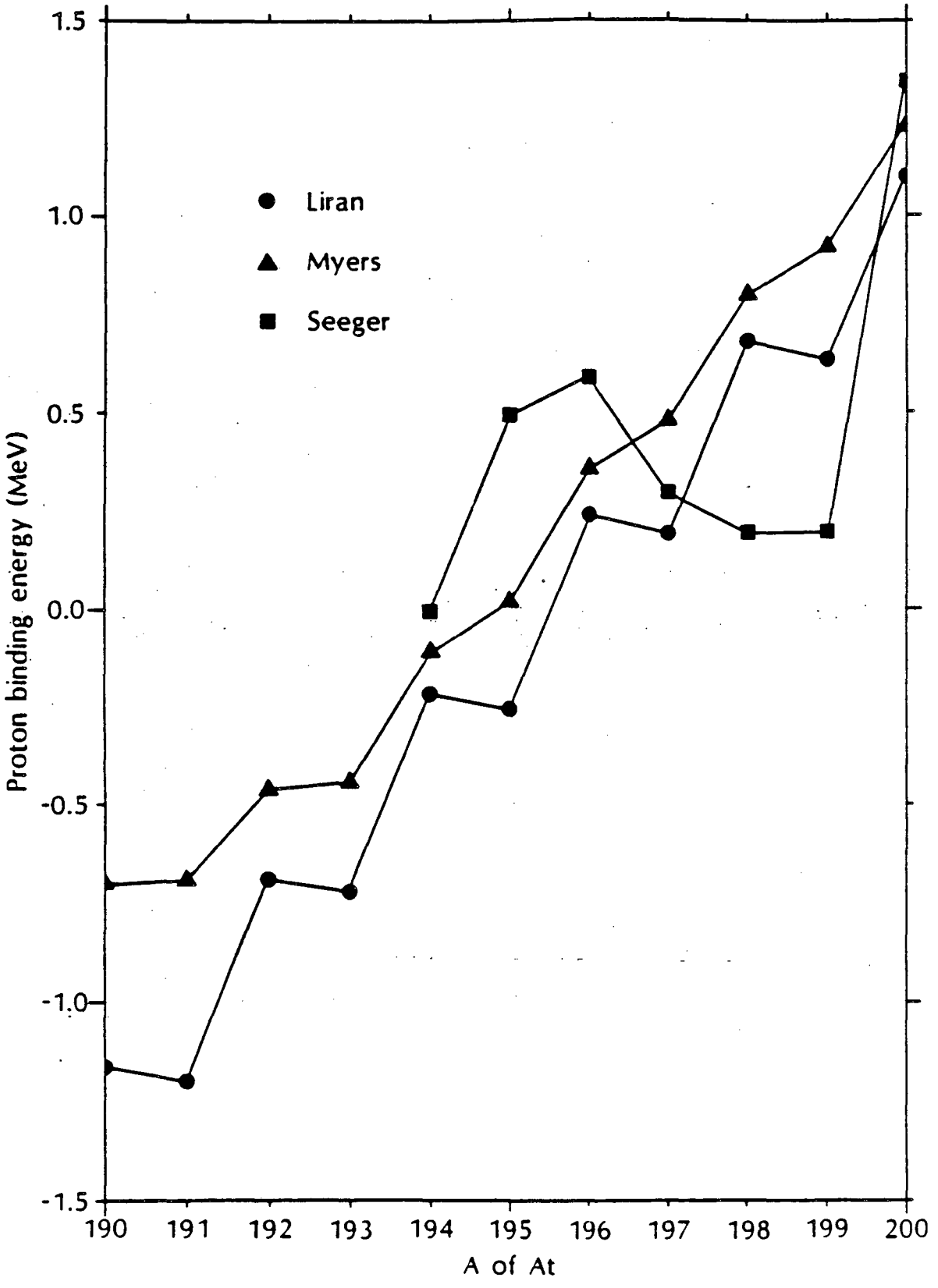
1.5
1.0
0.5
0.0
-0.5
-1.0
-1.5
Proton binding energy (MeV)
Liran
Myers
Seeger
190
191
192
193
194
195
196
197
198
199
200
A of At

Fig. 19

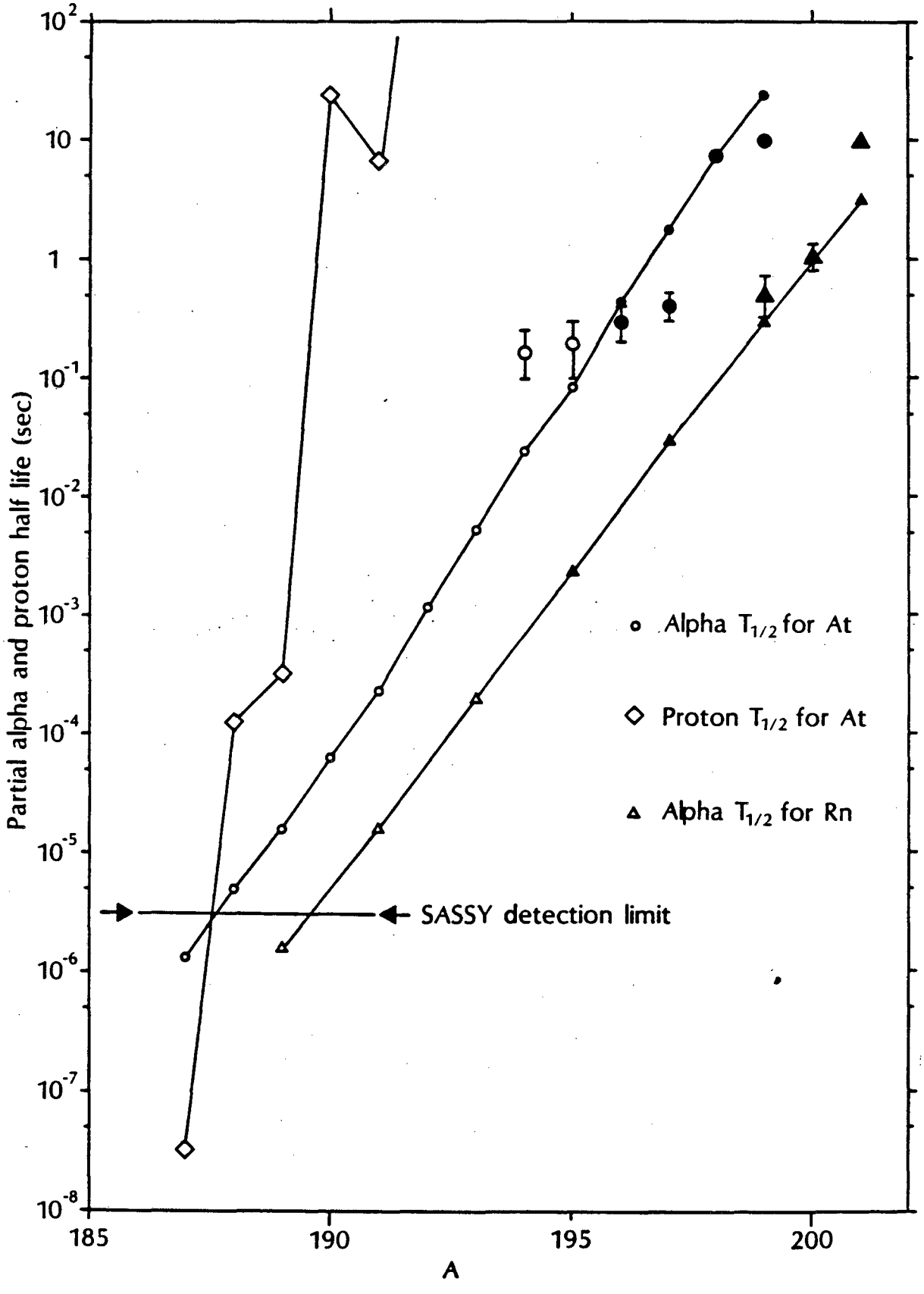
Partial alpha and proton half life (sec)
10^{2}
10
1
10^{-1}
10^{-2}
10^{-3}
10^{-4}
10^{-5}
10^{-6}
10^{-7}
10^{-8}
185
190
195
200
A
Alpha $T_{1/2}$ for At
Proton $T_{1/2}$ for At
Alpha $T_{1/2}$ for Rn
SASSY detection limit

Fig. 20

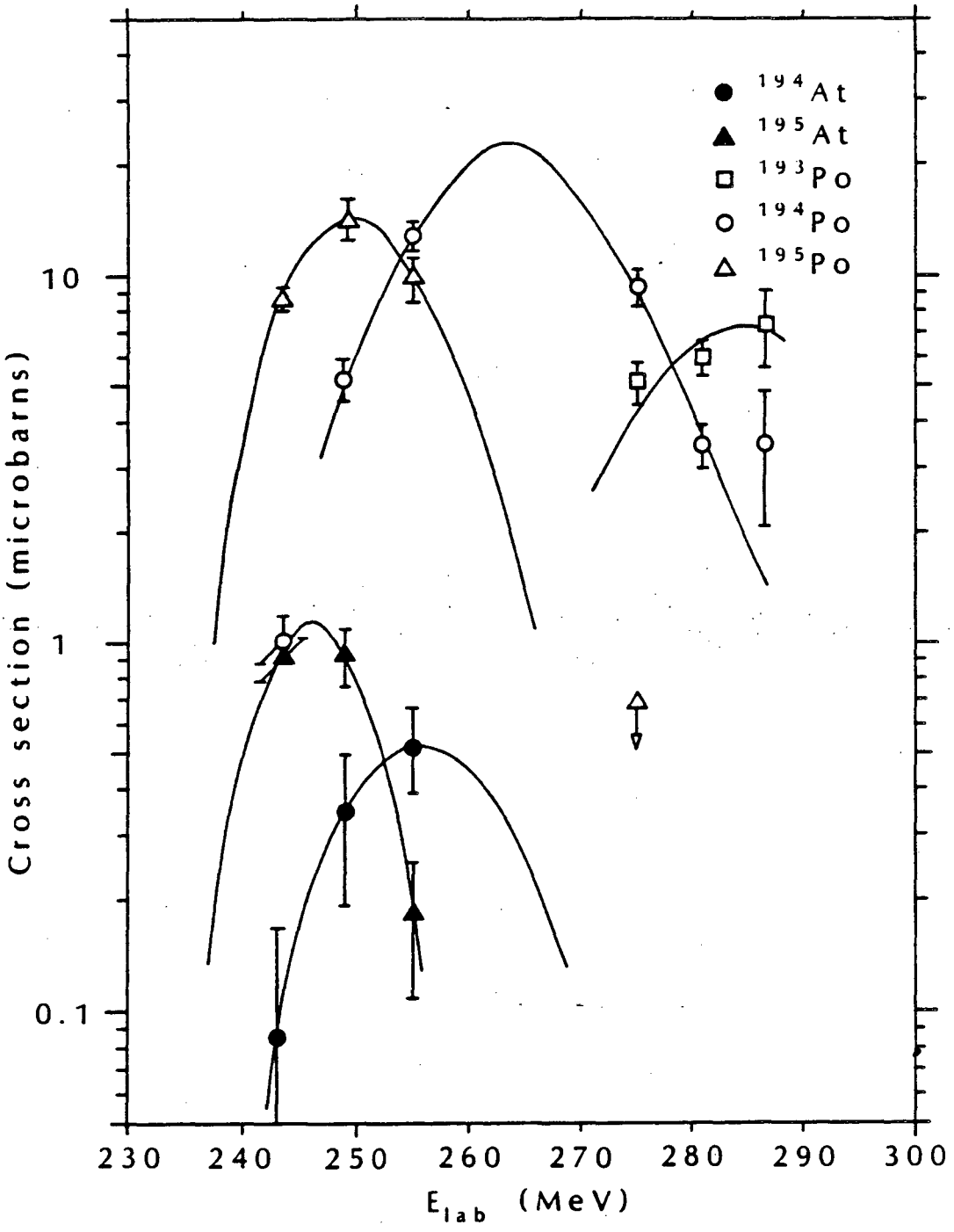
^{194}At
^{195}At
^{193}Po
^{194}Po
^{195}Po
Cross section (microbarns)
10
1
0.1
230
240
250
260
270
280
290
300
E_{lab} (MeV)

Fig. 21

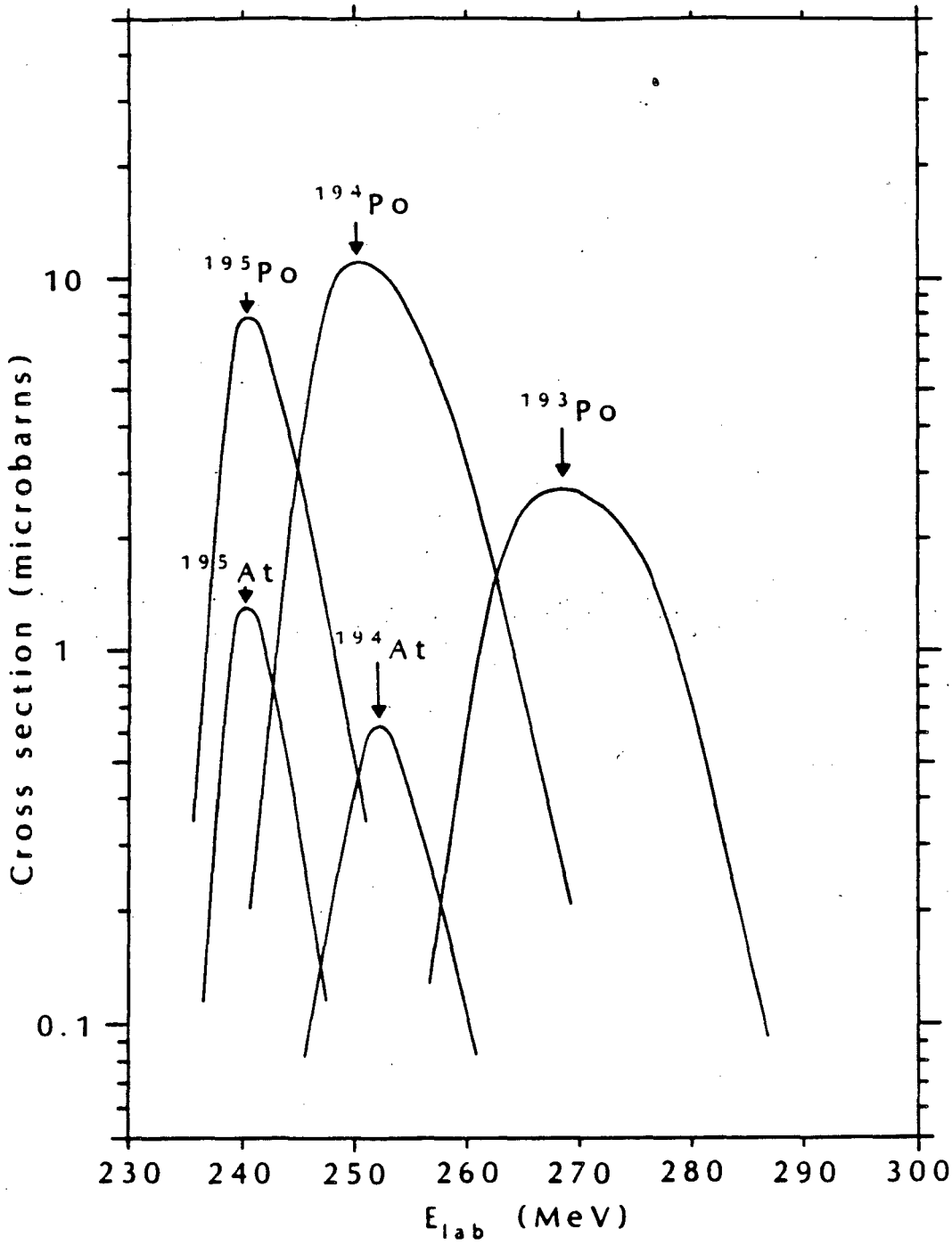
Cross section (microbarns)
10
1
0.1
230
240
250
260
270
280
290
300
E lab (MeV)
194 Po
195 Po
193 Po
195 At
194 At

Fig. 22

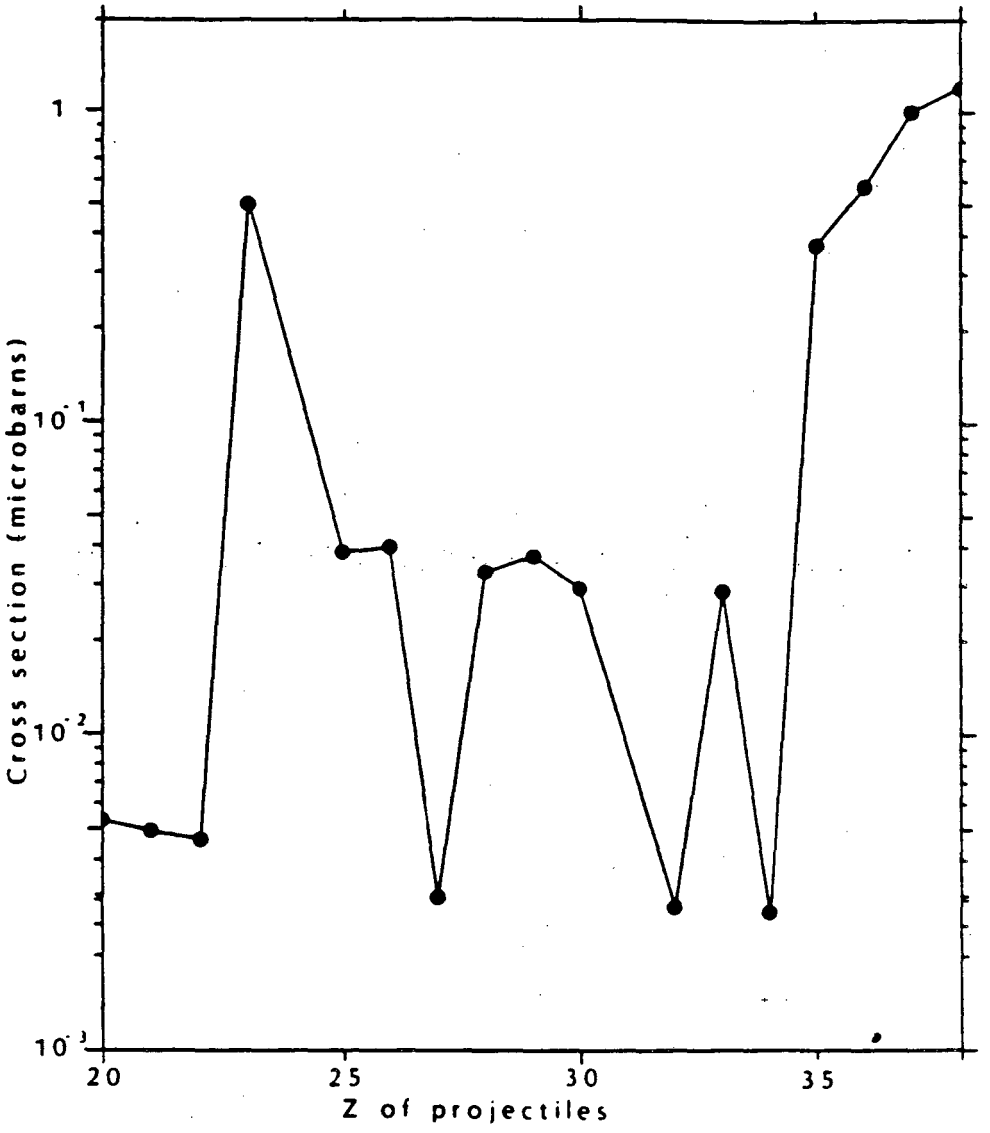
Cross section (microbarns)
1
10^{-1}
10^{-2}
10^{-3}
20
25
30
35
Z of projectiles

Fig. 23

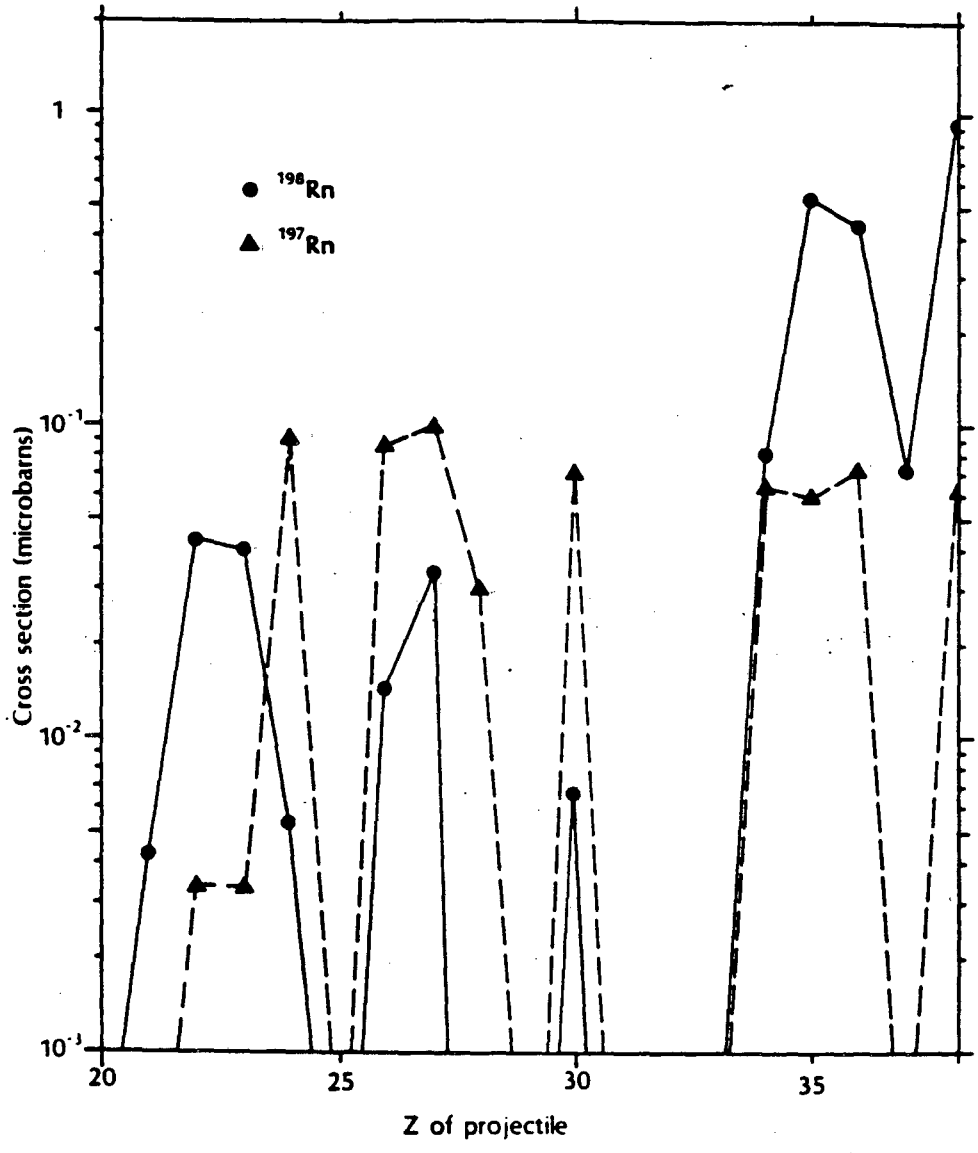
1
10^{-1}
10^{-2}
10^{-3}
Cross section (microbarns)
^{198}Rn
^{197}Rn
20
25
30
35
Z of projectile

Fig. 24

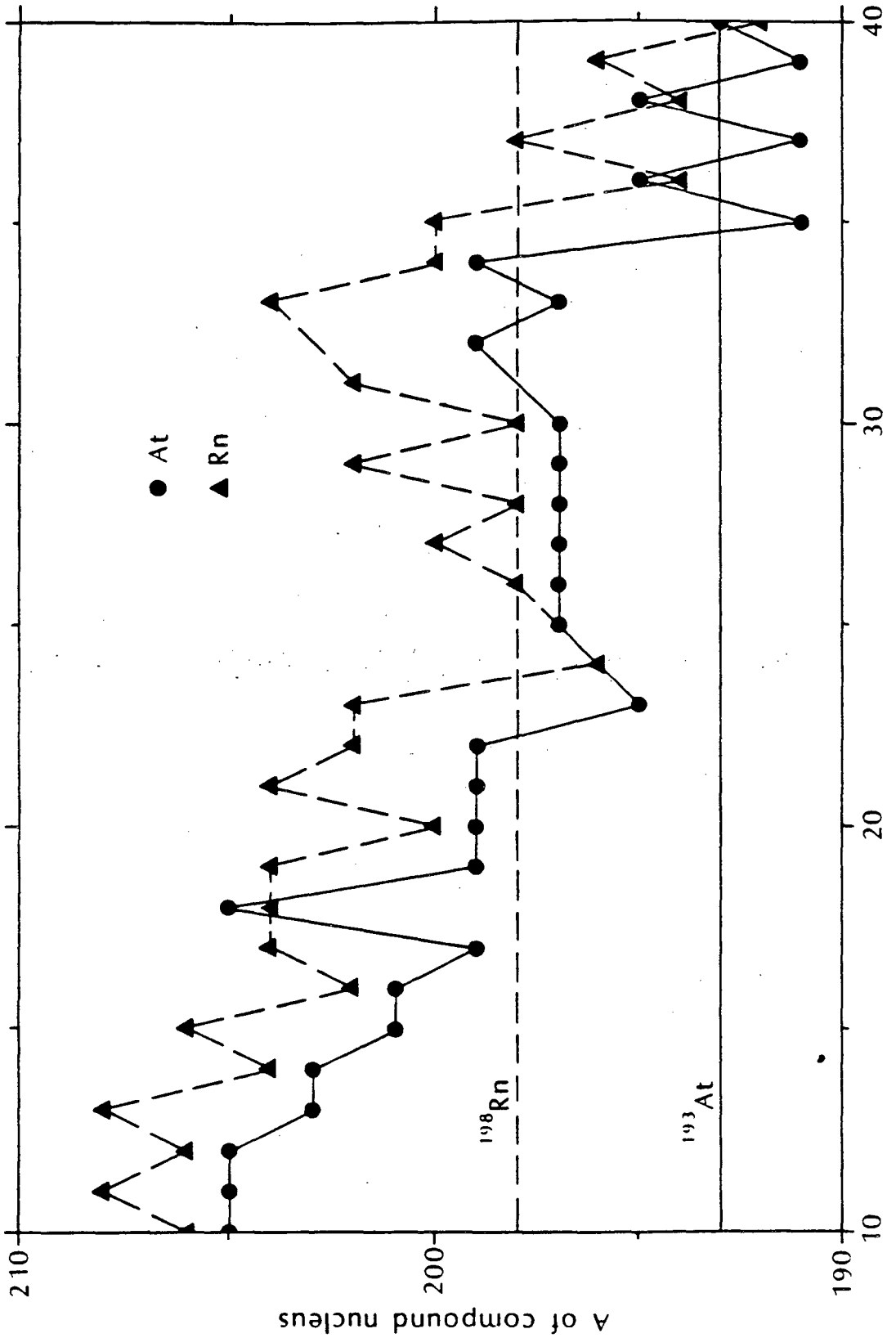
A of compound nucleus
210
200
190
10
20
30
40
Z of projectiles
At
Rn
^{198}Rn
^{193}At

Fig. 25

TECHNICAL INFORMATION DEPARTMENT
LAWRENCE BERKELEY LABORATORY
UNIVERSITY OF CALIFORNIA
BERKELEY, CALIFORNIA 94720